BLANKET ENGINEERING

KEYWORDS: *fusion neutronics experiments, fusion blanket, tritium breeding*

THE NUCLEAR ANALYSIS OF AN ANNULAR Li_2O BLANKET SYSTEM SURROUNDING AN ARTIFICIALLY SIMULATED 14-MeV LINE SOURCE AND COMPARISON OF CALCULATIONS TO MEASUREMENTS

M. Z. YOUSSEF, M. A. ABDOU, A. KUMAR, and LI ZHANG
University of California, Los Angeles, School of Engineering and Applied Science
Mechanical, Aerospace, and Nuclear Engineering Department
Los Angeles, California 90095

K. KOSAKO, Y. OYAMA, F. MAEKAWA, Y. IKEDA, C. KONNO, and H. MAEKAWA *Japan Atomic Energy Research Institute*
Department of Reactor Engineering, Tokai Research Establishment
Tokai-mura, Naka-gun, Ibaraki-ken 319-11 Japan

Received January 28, 1994
Accepted for Publication July 28, 1994

Experimental simulation to a line source has been realized at the Japan Atomic Energy Research Institute (JAERI) Fusion Neutronics Source within the U.S. Department of Energy/JAERI collaborative program on fusion neutronics. This simulation, achieved by cyclic movement of an annular Li_2O test assembly relative to a stationary point source, was a step forward in better simulation of the energy and angular distributions of the incident neutron source found in tokamak plasmas. Thus, compared with other experiments previously performed with a stationary point source, the uncertainties (that are system dependent) in calculating important neutronics parameters, such as tritium production rate (TPR), will be more representative of those anticipated in a fusion reactor. The rectangular annular assembly used is 1.3 × 1.3 m and 2.04 m long with a square cavity of 0.42 × 0.42 m cross section where the simulated line source (2 m long) is located axially at the center. To characterize the incident neutron source, flux mapping with foil activation measurements was performed in the axial direction (Z = −100 cm to Z = 100 cm) at the front surface of the assembly in the cavity with the annular blanket in place, and comparison was made to the bare line-source case (without annular blanket). Three phases of experiments were performed. In Phase-IIIA, a 1.5-cm-thick stainless steel first wall was used. An additional 2.45-cm-thick carbon layer was added in Phase-IIIB, and a large opening (42.55 × 37.6 cm) was made at one side at the center of the annular assembly in Phase-IIIC. Calculations were performed independently by the United States and JAERI for many measured items that included TPR from $^6Li(T_6)$, $^7Li(T_7)$, in-system spectrum measurements, and various activation measurements. In this paper, the calculated-to-measured values for the aforementioned measured items are given, as obtained separately by the United States and JAERI. In addition, the mean value of the prediction uncertainties of the local and line-integrated TPR and the associated standard deviations are given based on the calculational and experimental results obtained in all the experiments.

I. INTRODUCTION

Phase III fusion integral experiments were conducted at the Fusion Neutronics Source (FNS) facility at the Japan Atomic Energy Research Institute (JAERI) within the U.S. Department of Energy (U.S. DOE)/JAERI Collaborative Program on Fusion Blanket Neutronics. Unlike other phases of the program in which

a 14-MeV point source was utilized (Phase I: open geometry,[1-3] Phase II: closed geometry[4-12]), a simulated line source has been utilized by moving an annular blanket assembly in a periodic motion relative to a stationary 14-MeV point source and thereby generating the same neutronics characteristics in the test assembly that would have been achieved by a true line source.[13-15] This simulation is a first-of-its-kind and opens new areas in advancing fusion neutronics research and development. Another major difference between Phase III experiments[14-19] and other experiments performed previously in Phases I and II is that the annular assembly totally surrounds the simulated line source. This leads to more prototypical conditions for the incident neutron source in terms of energy and angular dependence resulting from the spatial dependence of the line source (versus a point source). These conditions are closer to those found in the toroidal plasmas in tokamaks.

The simulation of the line source has been achieved at JAERI through two modes of operation, namely the stepwise mode and the continuous mode of operation. In the former, the D-T neutrons are generated at a selected number of points along the simulated line source. These point sources are equally separated from each other and the duration of operating the D-T neutron source is equal at each point. In the latter operation mode, the annular assembly moves continuously relative to the fixed point source in a periodic movement with a speed of 6.1 mm/s. It was shown that both modes of operation produce the same neutronics effects inside the assembly.[14,15] Several measurements have been performed for tritium production rate, spectra, and several reaction rates, and the calculated results were compared to the experimental values to examine the prediction accuracies obtained by various codes and databases. Both JAERI and the U.S. have separately performed these analyses using their own computational tools and neutron databases.

The subject of this paper is to discuss the analyses and quantify the prediction uncertainties of the measured parameters. The impact of design variations (e.g., inclusion of a carbon layer, large opening, etc.) on the profiles of tritium production rates (TPR) is also emphasized. Furthermore, the prediction uncertainties in the local as well as the line-integrated TPR are estimated based on the calculational and experimental uncertainties (errors) at each location where TPR is measured by various techniques. From these prediction uncertainties, the mean prediction uncertainties in TPR and the possible spread around these mean values are evaluated. For more detail about the description on the experimental techniques and measurements, the reader is referred to Refs. 15 through 21. The experiments are briefly described in Sec. II. Discussion of the calculational methods applied by the U.S. and JAERI is given in Sec. III. The analytical results and the comparisons with the experimental values are given in Sec. IV. Section V is devoted to estimating the overall prediction uncertainties in the local and line-integrated TPR. Conclusions from this work are outlined in Sec. VI.

II. THE EXPERIMENTS

Figure 1 shows the experimental annular assembly of 2040-mm length and outer dimensions of 1301 mm × 1301 mm (see also Ref. 17 for other details). The inner cavity has a square shape of 425.5 mm × 425.5 mm with a 15-mm-thick Type 304 stainless steel first wall (FW). The Li_2O zone is 203 mm thick followed by a 203-mm-thick Li_2CO_3 zone whose outer surface is covered by a 16-mm polyethylene (PE) layer to isolate the assembly from the room-returned neutrons. Both ends of the assembly are open to facilitate its movement relative to the long-tube water-cooled neutron target. The length of the simulated line source is 2000 mm. There are six experimental drawers (in Phase IIIA and IIIB) in the radial direction (three on each side) that are filled with special blocks of Li_2O and Li_2CO_3 separated by ~509 mm. In the Phase IIIB experiment, a 2.54-cm-thick layer of carbon was placed in front of the FW, to act as an armor zone used in fusion reactors. The measurements were repeated to study the impact of the armor inclusion on the neutronics characteristics of the test assembly. In the Phase IIIC experiment, a large opening of 376-mm × 425.5-mm dimensions was made at one side at the center of the annular assembly of Phase IIIB, as shown in Fig. 2. This opening simulates the ports and ducts in a fusion reactor that are necessary for vacuum pumping, plasma diagnostics, neutral beam injection, etc. There are three drawers facing the opening on the other side of the assembly (drawers A & B & C) and a drawer (D) next to the opening in the radial direction. The objective of the Phase IIIC experiment is to experimentally and analytically (using three-dimensional transport codes) verify the effect of the inclusion of a large opening on the tritium production characteristics in the test assembly. Since the coverage fraction of the opening in Phase IIIC relative to the full coverage case of Phase IIIB is not negligible, it is expected that total tritium production rates and their profiles will be decreased due to (a) the removal of part of the breeding zone itself and (b) the decrease in the reflected component of the incident source neutron due to the existence of the large opening.

Prior to performing the in-system measurements, the simulated line source was characterized without the annular assembly in place. This was performed by measuring several activation reactions in the axial direction ($Z = -100$ cm to $Z = 100$ cm) and at a distance of 219 mm from the line source. The continuous operation mode was adopted for these measurements and the multifoils (MF) were placed at eleven positions that are 200 mm apart. These measurements were also made with the assembly placed around the line source and

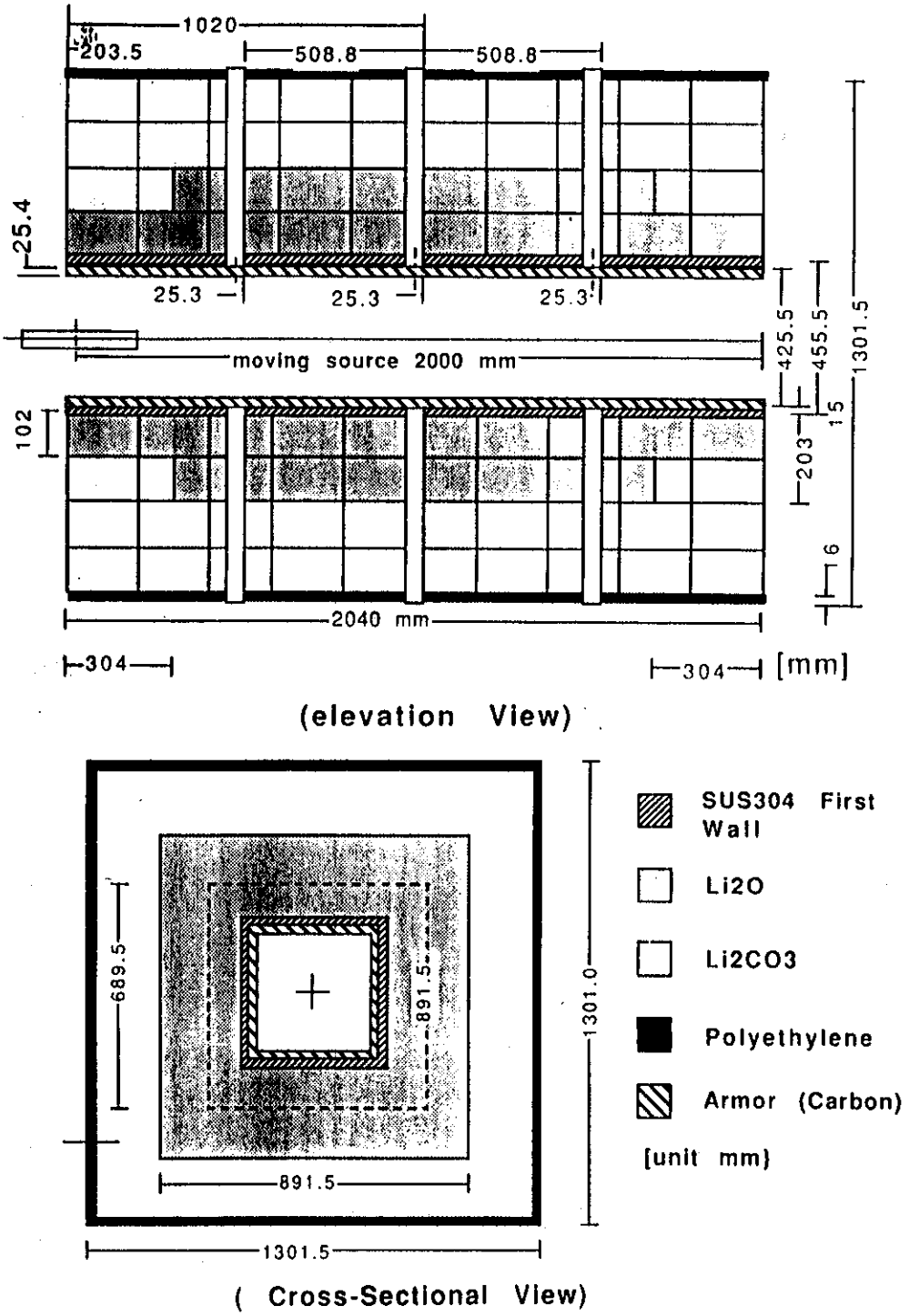

Fig. 1. Experimental arrangement for the Phase IIIB experiments.

comparisons were made to the without-the-assembly case. Performing this task was necessary to study the impact of the reflected neutrons traveling inside the inner cavity on these MF activation measurements. The experiments were performed in the first target room of the FNS facility which is large (~15 m × ~15 m × 9 m) compared to target room #2 (~5 m × ~5 m × 5 m) where previous experiments in Phase I through II were performed. The consequence is that the component of the room-returned neutrons in Phase III experiments is small and do not adversely affect the in-system measurements. For the bare source characteristics experiments, however, it is expected to find a large discrepancy between calculations and measure-

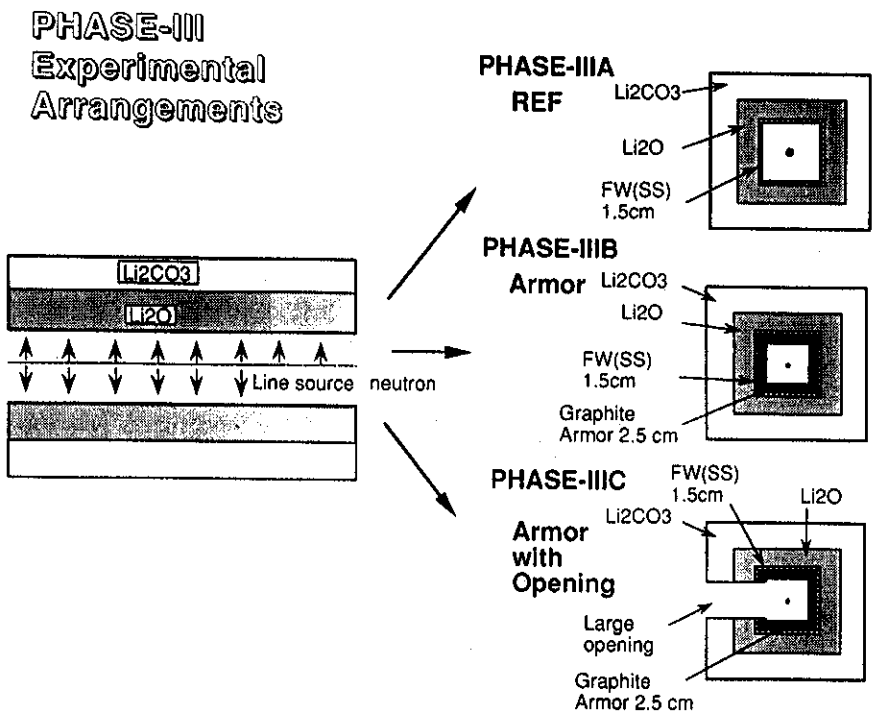

Fig. 2. Experimental arrangement for the Phase III experiments.

ments for nonthreshold reactions such as $^{197}Au(n,\gamma)$, where reflection from the room floor (at a distance of ~3 m) is large and will cause this discrepancy, unless the calculational model takes into account the floor and other equipment located close to the assembly. The reactions considered to characterize the source in the continuous mode of operation include: $^{58}Ni(n,2n)^{57}Ni$, $^{90}Zr(n,2n)^{89}Zr$, $^{93}Nb(n,2n)^{92m}Nb$, $^{27}Al(n,\alpha)^{24}Na$, $^{56}Fe(n,p)^{56}Mn$, $^{59}Co(n,\alpha)^{56}Mn$, $^{58}Ni(n,p)^{58}Co$, $^{64}Zn(n,p)^{64}Cu$, and $^{115}In(n,n')^{115m}In$. These reactions have effective threshold energies of ~13 MeV, ~12 MeV, ~8 MeV, ~6 MeV, ~5 MeV, ~5 MeV, ~2 MeV, ~2 MeV, and ~0.5 MeV, respectively. Also, the nonthreshold reaction $^{197}Au(n,\gamma)$ was considered as an index for the thermal neutrons.

Neutron spectra above 1 MeV along the central axis of the three drawers was measured by the NE213 detectors at four locations each. A proton recoil counter (PRC) was used to measure neutron spectrum in the energy range of a few keV to 1 MeV at the inner surface of the cavity and at a distance of 5 cm inside the Li_2O zone for the stepwise mode of operation. Li-glass detectors were used to measure the tritium production rate from $^6Li(T_6)$ inside the drawers, while the NE213 indirect method was used to measure the tritium production rate from $^7Li(T_7)$ by folding the measured spectrum with the $^7Li(n,n'\alpha)t$ cross section from JENDL-3PR2. The T_6 and T_7 were also measured inside the drawers in the continuous operation mode (long irradiation time of ~10 h) by using Li_2O pellet technique.

III. CALCULATIONAL METHODS

Both deterministic and Monte Carlo methods were used to analyze the experiments. The U.S. adopted the DOT5.1 code[22] along with the RUFF (Ref. 23) first collision code for the deterministic treatment while the MCNP-3B code that uses continuous energy and angle ENDF/B-V data was applied in the Monte Carlo treatment. The cross-section library used in DOT5.1 calculations (P_3-S_{16}) is the 30-group MATXS5 library,[24] which is based on ENDF/B-V (version 2) data. In JAERI's analysis, the DOT3.5 code was applied in the deterministic method along with the FNSUNCL code. The latter is a modified version of GRTUNCL (Ref. 25) in which multiple neutron sources, including variations in energy and angular distributions, were considered. The FNSUNCL is thus equivalent to the RUFF code. The FUSION-J3 library (P_5-S_{16}, 125-n, 41-g) based on JENDL-3 data was used in the DOT3.5 calculations. For the Monte Carlo calculations, the MORSE-DD (Ref. 26) code and the GMVP (Ref. 27) code (a vectorized version of MORSE-DD) were applied along with the DDXLIBJ3 library (125-g, double differential cross-section library based on JENDL-3).

In the two-dimensional calculations performed by DOT5.1 (U.S.), the energy and angular distribution of neutrons generated at the D+ beam spot on the Ti-T target was treated relativistically. It was necessary to perform first a three-dimensional MCNP calculation

for the long tube water-cooled target in order to account for the presence of the target structure and coolant tubes and thus generate the appropriate angular/energy distributions of the incident neutrons in the annular assembly. These distributions were assumed at each of the point source locations considered in the simulation of the line source, and a single RUFF run was made to estimate the first collision neutron source needed for the DOT5.1 calculations. Notice in this approach that while neutron collisions in the target structure and coolant channels are considered in the initial MCNP run, neutrons that reach the annular assembly and reflect back to the target to interact with its structure and reflect back to the annular assembly are ignored, i.e., interactions in the annular assembly and the target structure are decoupled. This decoupling was necessary, otherwise a separate RUFF/DOT run would have been performed at each selected point source to account for the varied length of the drift tube inside the cavity as one moves toward the front edge of the assembly (details of the drift tube and target structure can be found in Refs. 16, 17, and 18). Similar procedures were applied in JAERI's DOT3.5/FNSUNCL calculations. The number of equally-spaced point source locations, N, selected for the line source simulation was 26 in the U.S. calculations and 41 in JAERI's calculations. It was shown that $N \sim 20$ is sufficient for the simulation.[13] The two-dimensional R-Z cylindrical model used for the deterministic methods calculations can be found in Ref. 28.

In the Monte Carlo treatment, there is no need for the multiple point source approach used in the DOT calculations. Random sampling of the energy and angular distributions of incident neutrons to the annular assembly for each position along the line source is made (continuously in MCNP calculations and from bins in the MORSE-DD calculations) from the distributions obtained from the initial Monte Carlo run for the drift tube/target calculations. The atomic densities of the materials used to construct the assembly are given in Table I.

IV. CALCULATIONAL RESULTS AND COMPARISON TO MEASUREMENTS

Figure 3 shows the relative intensity of total neutrons emitted from the long tube water-cooled target (WCT) obtained from the initial Monte Carlo run (JAERI) for the drift tube/target alone (no assembly). Forward emitted neutrons ($0 < \mu \leq 1$) exceed the backward neutrons ($-1 \leq \mu < 0$) by ~10% due to reaction kinematics and collisions in the target assembly. Incident neutron spectra are shown in Fig. 4 in the direction $\mu = 1$, 0, and -1, where it peaks around 15 MeV for $\mu = 1$ and at 13.6 MeV for $\mu = -1$. In the latter case, more soft neutrons are found as compared to $\mu = 1$ and $\mu = 0$ cases due to the reaction kinematics for 330-keV deuteron acceleration.

IV.A. Source Characteristics

IV.A.1. Bare Source and Source with Annular Assembly (Phase IIIA)

Figure 5 shows the axial distribution in the Z direction (from Z = −100 cm to Z = 100 cm) at a radial distance R = 21.9 cm from the line source for the $^{58}Ni(n,2n)$ [E_{th} ~ 13 MeV], $^{27}Al(n,\alpha)$ [E_{th} ~ 6 MeV], and $^{115}In(n,n')^{115m}In$ reactions [E_{th} ~ 0.5 MeV] in the bare source case (without the assembly). The $^{58}Ni(n,2n)$ reactions are larger in the forward direction (Z > 0, toward the front end) relative to the values in the back direction (Z < 0; toward the back end on the target side). Locations that are toward the front end see more forward neutrons than backward neutrons as the target travels from Z = −100 cm to Z = 100 cm. As

TABLE I

Atomic Densities of Materials Used in Phase III Experiments*

Element	SS304	Li_2O[a]	Li_2CO_3	Polyethylene	Graphite
Fe	6.0210−2[b]	1.0976−3			
Cr	1.5302−2	3.0188−4			
Ni	8.2258−3	1.3358−4			
^{55}Mn	1.2607−3	1.5440−5			
^{6}Li		4.1921−3	2.2798−3		
^{7}Li		5.2411−2	2.8030−2		
^{16}O		2.8302−2	4.5464−2		
^{12}C			1.5155−2	4.1280−2	8.2894−2
H				8.2560−2	

*Given in atom/cm^3 × 10^{24}.
[a]Includes Type 304 stainless steel structure.
[b]Read as 6.0210 × 10^{-2}.

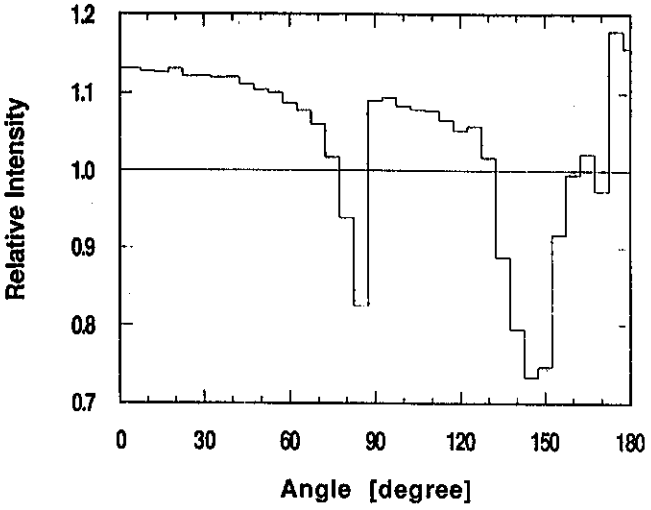

Fig. 3. Relative intensity of the incident neutron source from the long tube water-cooled target (JAERI's calculations).

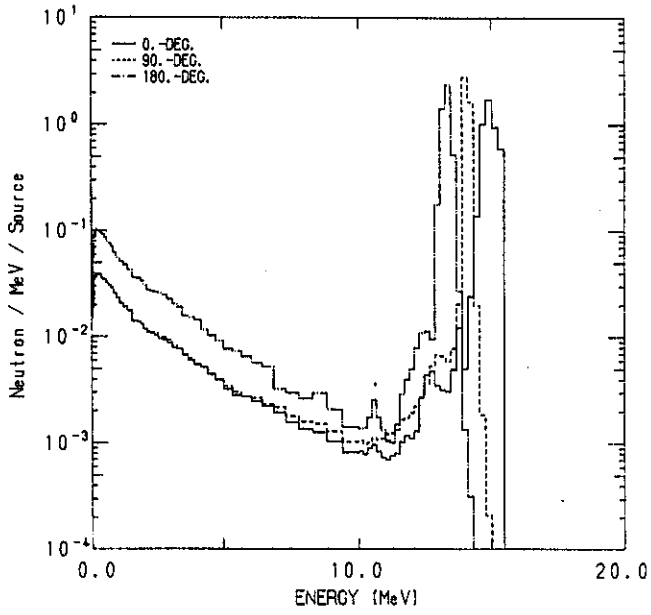

Fig. 4. Incident neutron spectrum from the long tube water-cooled target (JAERI's calculations).

shown in Figs. 3 and 4, these forward neutrons are larger by ~10% and also peak around 15 MeV where the $^{58}Ni(n,2n)$ cross-section is large. Reactions such as $^{115}In(n,n')$ have low threshold energies. Locations that are near the back end (target side) see more of backward emitted neutrons than forward emitted neutrons. The backward emitted neutrons ($\mu < 0$) are less than the forward ones (see Fig. 3); however, most of the backward neutrons have a larger low-energy neutron component above the threshold energy of the $^{115}In(n,n')$

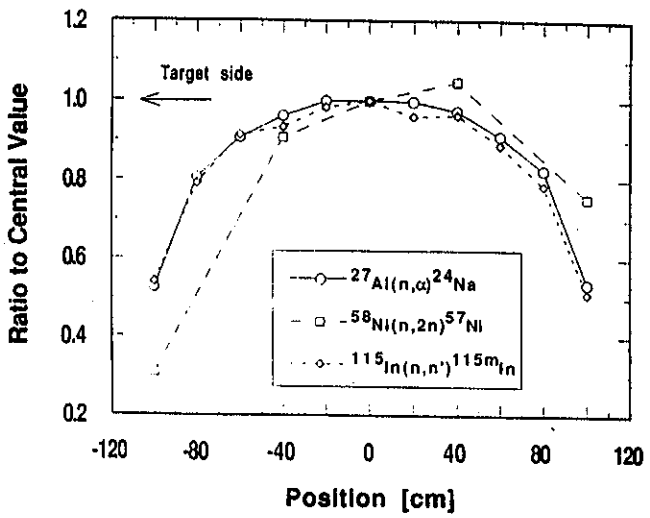

Fig. 5. Reaction rate distribution in the axial direction for $^{27}Al(n,\alpha)$, $^{58}Ni(n,2n)$, and $^{115}In(n,n')$ reactions at a radial distance R = 219 cm without the assembly (JAERI's measurements).

reactions, and this compensates for the intensity difference seen in Fig. 3 resulting in a more or less symmetric distribution relative to the central value at Z = 0.

The calculated-to-experimental value (C/E) for the high threshold reaction, $^{90}Zr(n,2n)^{89}Zr$, [E_{th} ~ 12 MeV] is shown in Fig. 6. The values are within 2 to 5% (MCNP, DOT3.5) and about −10% (DOT5.1). The C/E values for the $^{115}In(n,n')$ reaction are shown in Fig. 7. The values obtained by JAERI (DOT3.5) are within 5% of the measurements while they are within −18% to +10% in the U.S. calculations with the largest deviations occurring at the front and back ends. It was noticed for other low-threshold reactions that the C/E curves exhibit an ascending trend as one moves toward the front end (Z = 100 cm). This could be due to discrepancies in the calculated incident spectrum. It seems that the spectrum of the backward neutrons is harder than it should be in the U.S. calculations resulting in lower C/E values (below unity) at locations near the back end (target side) where neutrons seen at the detector locations are mostly backward. On the other hand, at locations near the front end, the larger C/E values (larger than unity) could be due to a softer spectrum for the forward neutrons than it should be in the U.S. calculated incident neutron source. This combined effect results in the ascending trends for the $^{115}In(n,n')^{115m}In$ reaction seen in Fig. 7 and for other low-threshold reactions [e.g., $^{58}Ni(n,p)$].

The presence of the assembly around the simulated line source resulted in an appreciable fraction of low-energy neutrons inside the cavity attributed to neutrons that are reflected by the assembly materials. It was shown[28] that an increase by a factor of 3 occurs in the $^{115}In(n,n')$ reaction at the inner surface of the cavity

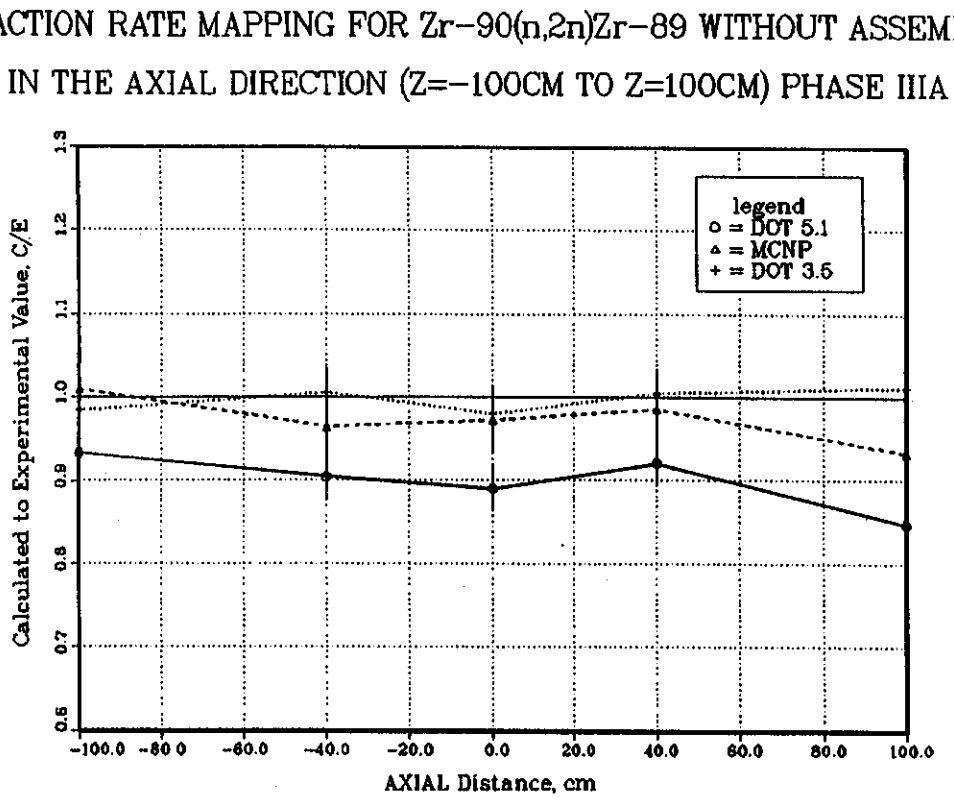

Fig. 6. The C/E values for the $^{90}Zr(n,2n)^{89}Zr$ reaction in the axial direction (without assembly).

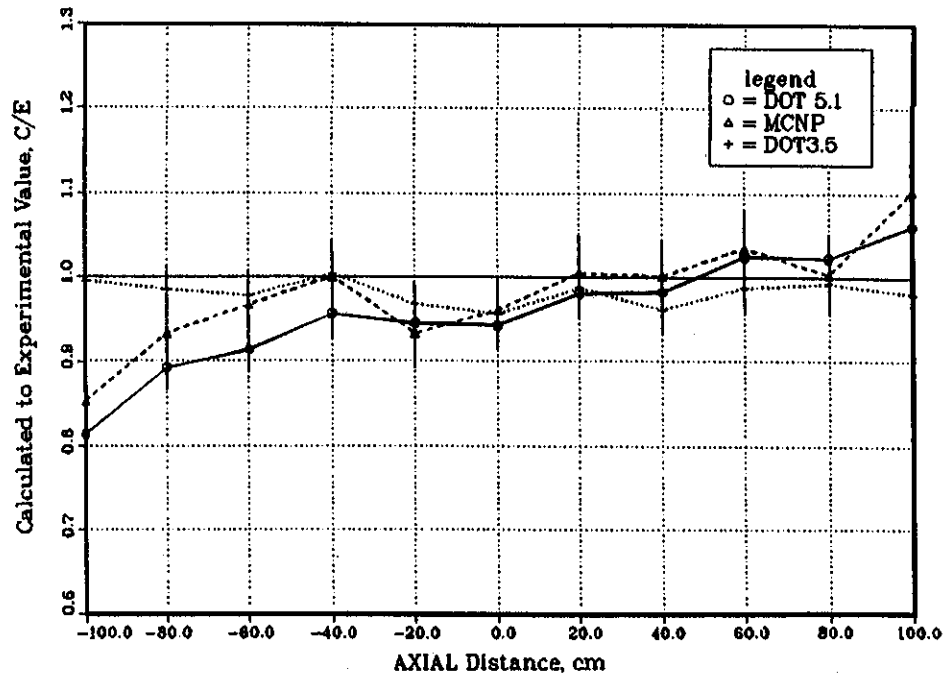

Fig. 7. The C/E values for the $^{115}In(n,n')^{115m}In$ reaction in the axial direction (without assembly).

at an axial distance Z = 0 for the cases with and without the annual assembly. Figure 8 shows the C/E values for the $^{93}Nb(n,2n)^{92}Nb$ reactions with the assembly in place. At most locations, the errors are overlapping. (Note: Errors in the Monte Carlo calculations include both the statistical calculational errors and the experimental errors. Errors in the DOT calculations are only the experimental errors.) The ascending trends in the C/E values obtained by the U.S. that are observed for the low-threshold reactions still persist but to a lesser extent, especially for these reactions that have relatively high threshold energies [e.g., $^{27}Al(n,\alpha)$]. The C/E values obtained by the DOT3.5 calculations (JAERI) are always larger than those obtained by the MORSE-DD code by 10 to 15% for the low energy response reactions and by ~5 to 10% for some (n,p) reactions that have relatively large threshold energies [e.g., $^{56}Fe(n,p)^{56m}Fe$, $E_{th} \sim 5$ MeV].

As for the nonthreshold reaction $^{197}Au(n,\gamma)$, the C/E curves in the with-assembly case of Phase IIIA are shown in Fig. 9. All calculations underpredict the reaction by as much as 15 to 50%, depending on the location along the Z axis, and the discrete ordinates results are larger than those obtained by the Monte Carlo methods by ~10 to 15%. As mentioned earlier, the underestimation is due to the room returned component from the floor that is not accounted for in the modeling. The underestimation is much larger (C/E ~ 0.03) in the case of a bare line source.

IV.A.2. Effect of Armor Layer and Large Opening

The inclusion of the armor layer at the inner surface of the assembly tends to increase the low-energy component of the incident neutron source due to reflection by carbon. Consequently, measured reaction rates that have no threshold or low threshold energies are enhanced inside the cavity and at the front zone inside the test assembly. In Sec. IV.A.3 of Ref. 17, the reactions $^{93}Nb(n,2n)^{92m}Nb$, $^{115}In(n,n')^{115m}In$, and $^{197}Au(n,\gamma)^{198}Au$ are shown along the line source in the Z axial direction at the surface of the assembly (located at the radial direction of 187 cm). It was shown that the reaction rates in the armor case (Phase IIIB) are larger than

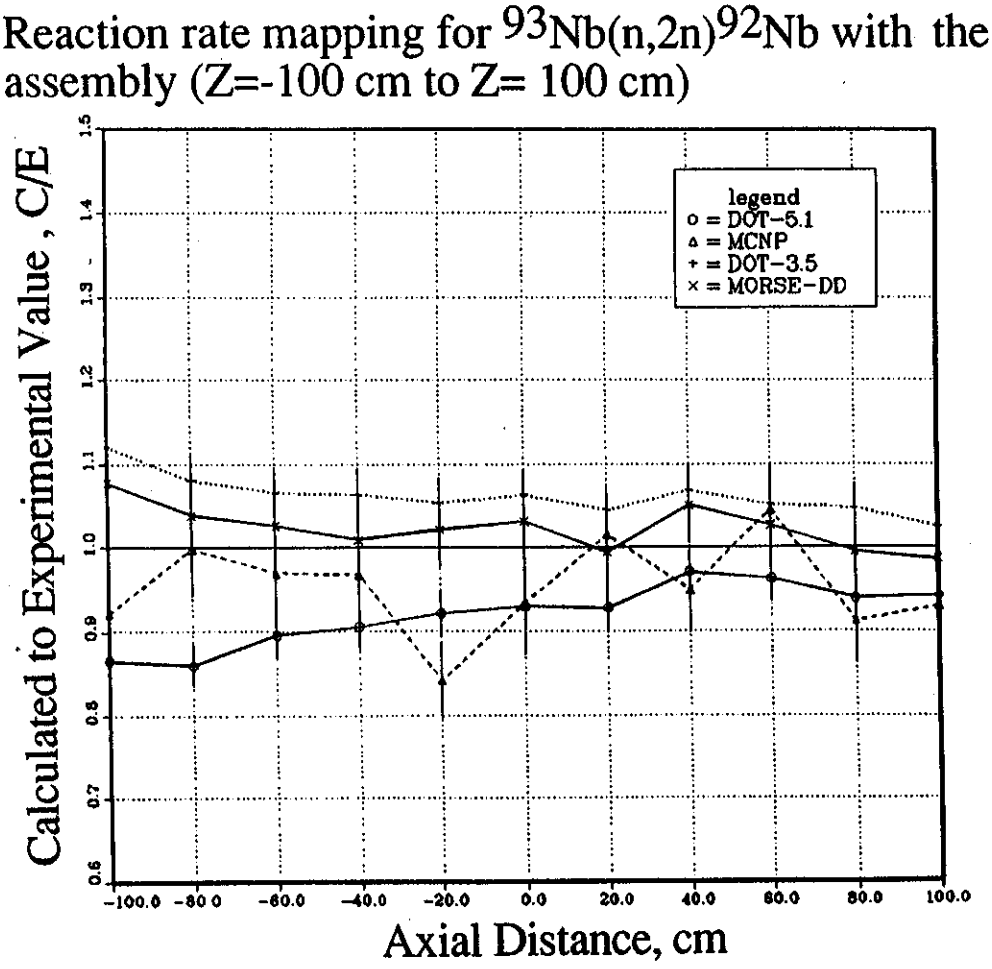

Fig. 8. The C/E values for the $^{93}Nb(n,2n)^{92}Nb$ reactions in the axial direction (with assembly), Phase IIIA.

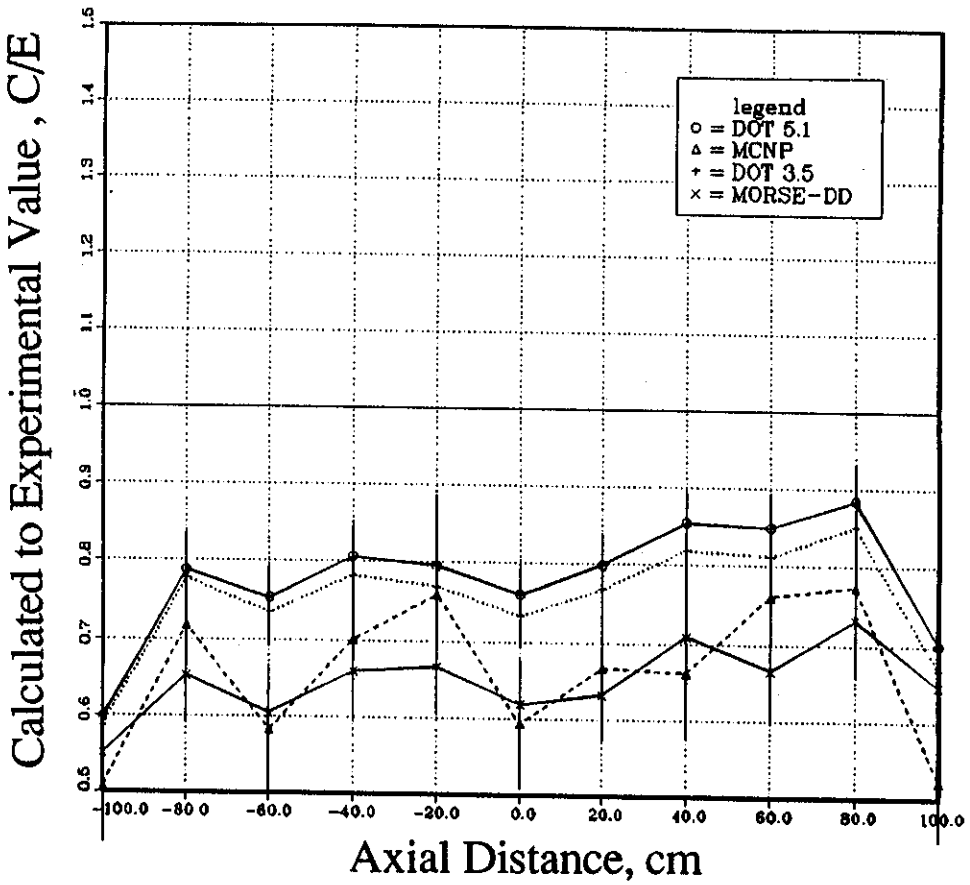

Fig. 9. The C/E values for the $^{197}Au(n,\gamma)^{198}Au$ reactions in the axial direction (with assembly), Phase IIIA.

those in the Phase IIIA reference case by ~19% and ~25% for the first two reaction rates and by a factor of ~4 for the $^{197}Au(n,\gamma)^{198}Au$ reaction. The increase is due to the shorter distance at which measurements were taken in Phase IIIB [particularly for the $^{93}Nb(n,2n)^{92m}Nb$ reaction] and large low-energy neutron component [particularly for the $^{197}Au(n,\gamma)^{198}Au$ reaction]. The effect of the opening of Phase IIIC is that a decrease occurs in the low-energy threshold reactions measured at the no-hole side (opposing side) of the test assembly and that decrease is noticeable along the whole region in the axial direction. In this latter phase, the reaction rates at the opening side relative to those at the opposite (no-opening) side are lower only around an axial width corresponding to the opening size (see Ref. 17). Figures 10, 11, and 12 show the C/E values for these reactions in Phase IIIB based on JAERI's analysis. Again, the DOT calculations give larger values than those obtained with the MORSE-DD code. However, the underestimation for the $^{197}Au(n,\gamma)^{198}Au$ reactions is not as pronounced in Phase IIIB as it is in Phase IIIA since the low-energy neutrons are increased due to the presence of the armor and the contribution of the room-returned background neutrons are relatively decreased. Generally the agreement between the JAERI's calculations for the several reaction rates considered without the assembly is within 5% while it is within 10% when the assembly is in place. Those obtained by the U.S. are within 10% (without the assembly) and within 10 to 20% (with the assembly).

IV.B. In-System Measurements

IV.B.1. Reaction Rates

Several multifoil activation rates were also measured along the axes of the radial drawers of Phase IIIA, IIIB, and IIIC. Numerical values of the measured reactions can be found in Ref. 17. Generally, the threshold-type reactions, such as $^{90}Zr(n,2n)^{89}Zr$, $^{93}Nb(n,2n)^{92m}Nb$, and $^{115}In(n,n')^{115m}In$, steadily decrease by depth inside the annular assembly in the radial direction, but the $^{197}Au(n,\gamma)^{198}Au$ reaction showed a flat profile except near the front surface. Upon the inclusion of the

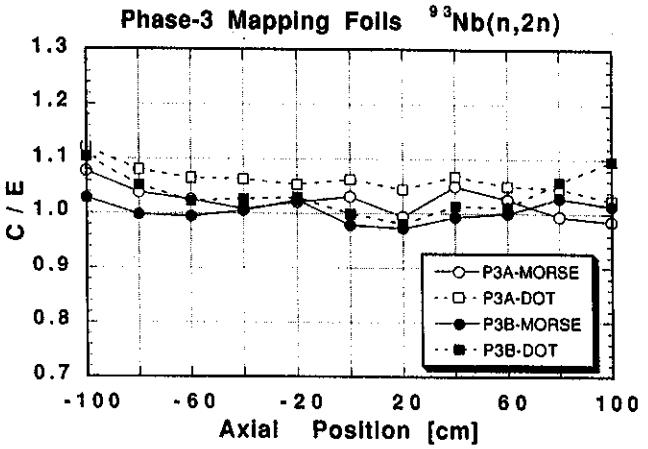

Fig. 10. The C/E values for the $^{93}Nb(n,2n)^{92}Nb$ reactions in the axial direction (Phase IIIA and IIIB).

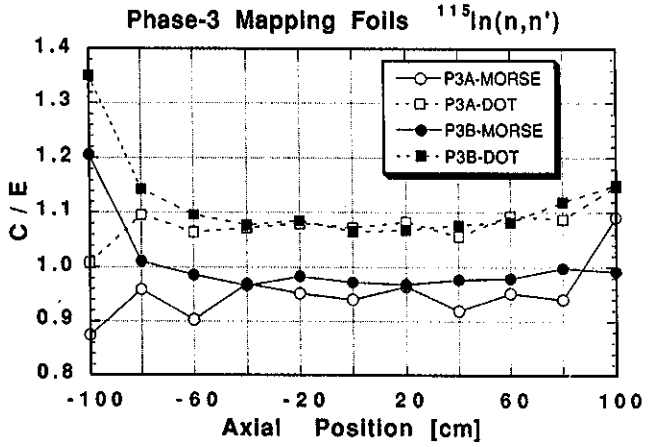

Fig. 11. The C/E values for the $^{115}In(n,n')^{115m}In$ reactions in the axial direction (Phase IIIA and IIIB).

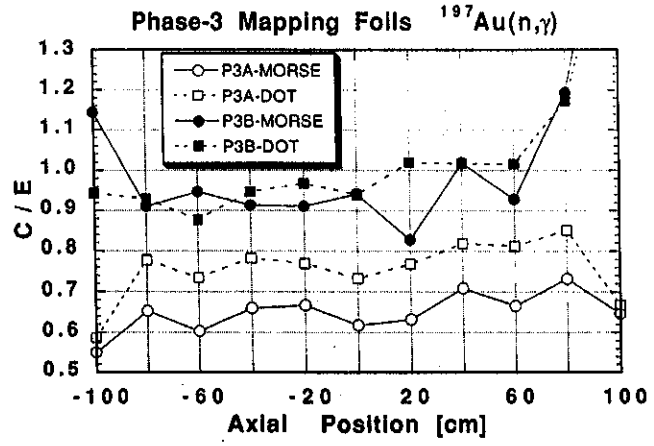

Fig. 12. The C/E values for the $^{197}Au(n,\gamma)^{198}Au$ reactions in the axial direction (Phase IIIA and IIIB).

armor layer, a decrease of ~10 to 30% occurs in the threshold-type reactions while the $^{197}Au(n,\gamma)^{198}Au$ reaction increased by ~ a factor of 2 at front locations in the assembly. There is practically no effect on the high-threshold reactions inside drawer B facing the opening in Phase IIIC as compared to Phase IIIB values, but the $^{197}Au(n,\gamma)^{198}Au$ reaction gets lower up to a depth of ~20 cm due to the decrease in the reflected low-energy neutrons upon the inclusion of the opening in Phase IIIC (Ref. 17).

Figure 13 shows the C/E value along the axis of drawer B in Phase IIIA for the $^{90}Zr(n,2n)^{89}Zr$ reactions. At the front surface of the cavity, the C/E values obtained by the U.S. are lower than those obtained by JAERI. However, the C/E values increase with increasing radial distance in the U.S. calculations and become greater than unity and those obtained by JAERI at deeper locations. Figure 14 shows the C/E values for the integrated spectrum above 10 MeV in drawer B of Phase IIIA. As shown, the integrated component is generally underestimated by all codes/data (in all drawers) and the values obtained by DOT5.1 (U.S.) are relatively the largest. The effect of this underestimation in the spectrum leads to lower values for the $^{90}Zr(n,2n)$ at the front locations, but the larger C/E values for this reaction at back locations, as obtained by the U.S., could be due to a combination of a relatively larger high-energy component of the spectrum and larger cross-section for that reaction. Figure 15 shows the C/E values for $^{115}In(n,n')^{115m}In$ reaction along the radial direction of drawer B of Phase IIIA. As was observed in the C/E curves in the axial Z direction, the discrete ordinates results of the U.S. and JAERI are, on the average, larger than the Monte Carlo results. This can also be seen in the C/E curves of the $^{93}Nb(n,2n)^{92m}Nb$, $^{115}In(n,n')^{115m}In$, and $^{197}Au(n,\gamma)^{198}Au$ reactions shown in Figs. 16, 17, and 18 (JAERI), where a comparison to Phase IIIB results can be made. The relatively larger results of DOT3.5 calculations are lessened at deeper locations compared to MORSE-DD results. The discrepancies between the two calculational methods are lessened in Phase IIIB. Note in particular that the C/E values for the $^{197}Au(n,\gamma)^{198}Au$ reaction are improved relative to the ones of Phase IIIA for the reasons mentioned earlier. In general, the features of the C/E curves for other reactions in the three phases are as follows: $^{27}Al(n,\alpha)$ is within 5% (JAERI) and 10% (U.S.); $^{58}Ni(n,p)$ is within 2 to 10% (JAERI) and 2 to 15% (U.S.); $^{93}Nb(n,2n)$ is <5% (JAERI) and 2 to 10% (U.S.), and for the $^{58}Ni(n,2n)$ reactions, the agreement is within 5% (JAERI) with a tendency to worsen toward the back locations.

IV.B.2. Neutron Spectrum

Figures 19 and 20 show a comparison between the spectrum calculated by DOT3.5 (JAERI) and measured by NE213 and PRC at the surface and at a depth of 79.4 mm from the FW (292.4 mm from the line source)

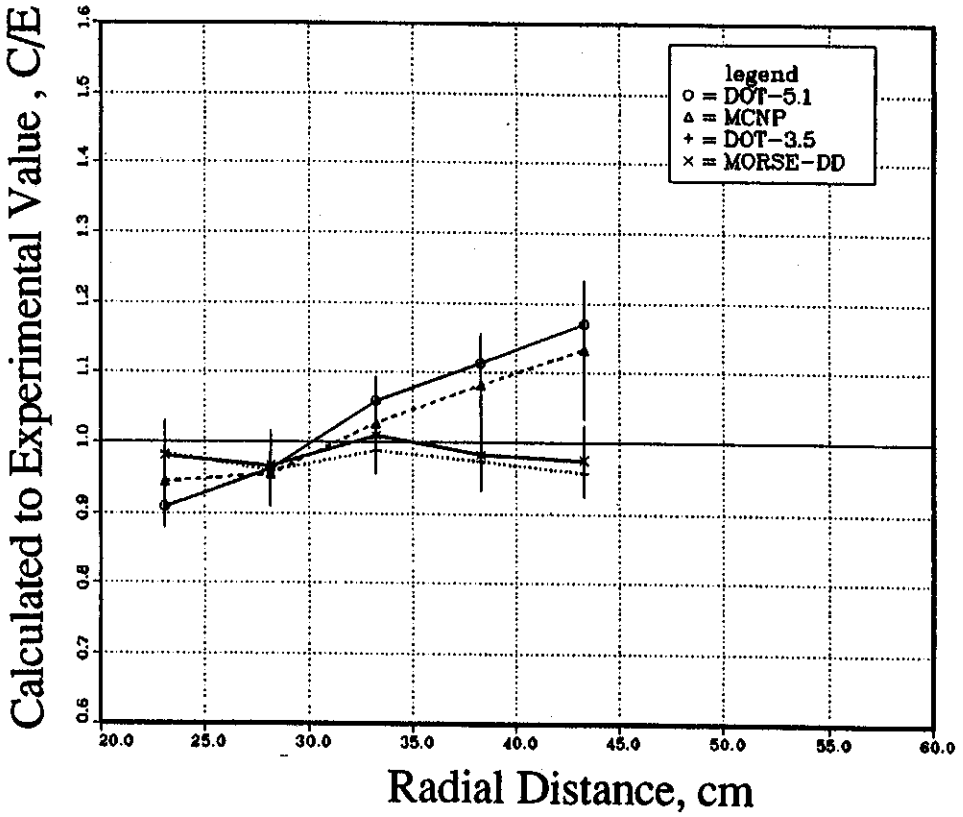

Fig. 13. The C/E values for the $^{90}Zr(n,2n)^{89}Zr$ reaction in the radial direction along drawer B, Phase IIIA.

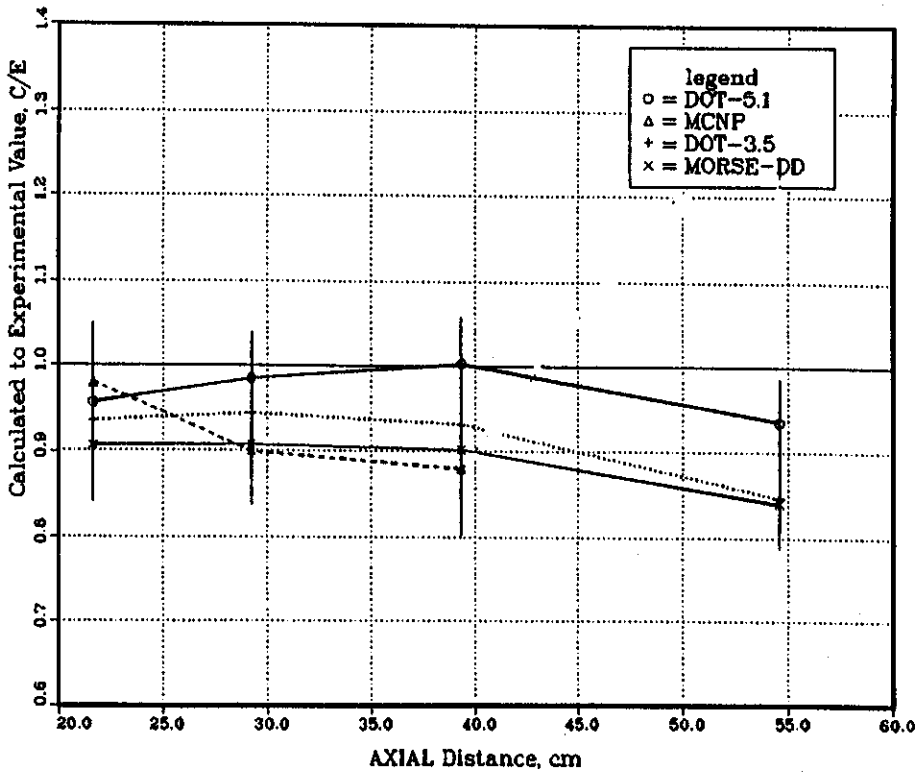

Fig. 14. Integrated neutron spectrum, E > 10 MeV, along the axis of drawer B, Phase IIIA.

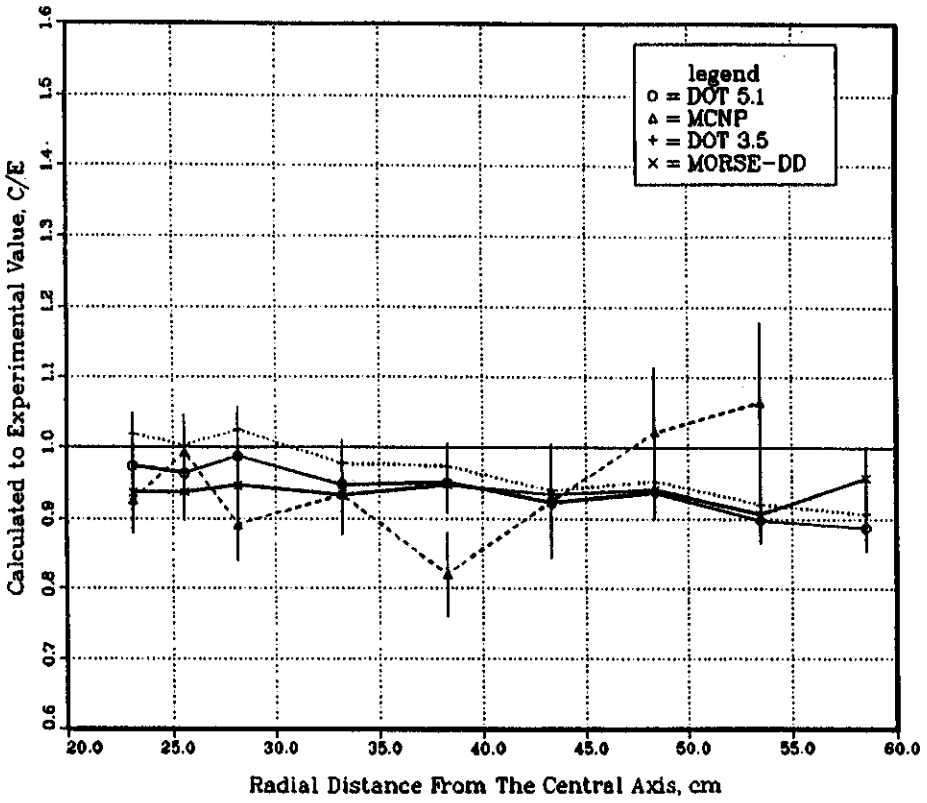

Fig. 15. The C/E values for the $^{115}In(n,n')^{115m}In$ reaction in the radial direction along drawer B, Phase IIIA.

of Phase IIIA. The two spectra are similar below 100 keV, except for the dip caused by resonance in iron at the surface. The dip caused by resonance in ^6Li at 250 keV is apparent in Fig. 20. It is clear that the peak of the uncollided flux is decreased inside the assembly, and generally ~50% decrease in the spectrum around 200 keV occurs at a depth 79.4 mm from the FW. A comparison between the surface spectrum and the spectrum at a depth of 79.4 mm from the FW in Phase IIIB is shown in Figs. 21 and 22. The similarity between the spectra at 79.4-mm depth is clear except for the larger dip in Phase IIIB at the 250-keV resonance of ^6Li. The agreement between the calculations and measured data is reasonable, as can be seen in Figs. 19 through 22. The C/E curves for the spectrum above 1 MeV measured by the NE213 detectors are shown in Fig. 23 based on the

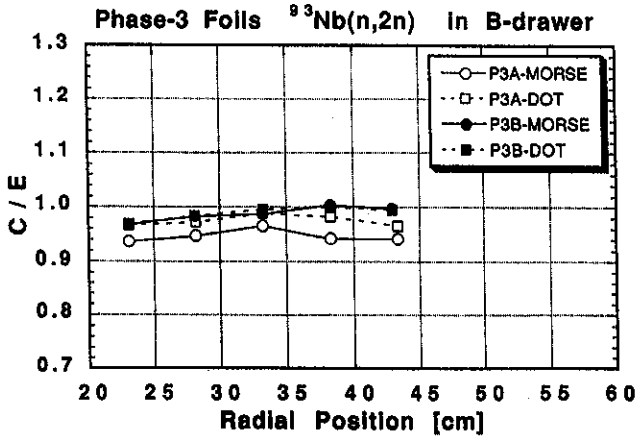

Fig. 16. The C/E values for the $^{93}Nb(n,2n)^{92}Nb$ reaction in the radial direction along drawer B, Phases IIIA and IIIB.

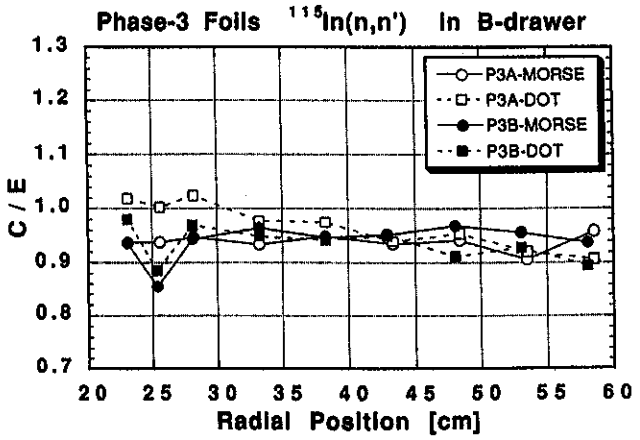

Fig. 17. The C/E values for the $^{115}In(n,n')^{115m}In$ reaction in the radial direction along drawer B, Phases IIIA and IIIB.

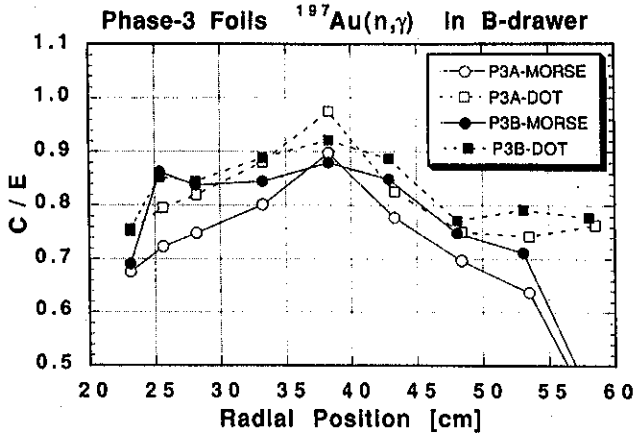

Fig. 18. The C/E values for the $^{197}Au(n,\gamma)^{198}Au$ reaction in the radial direction along drawer B, Phases IIIA and IIIB.

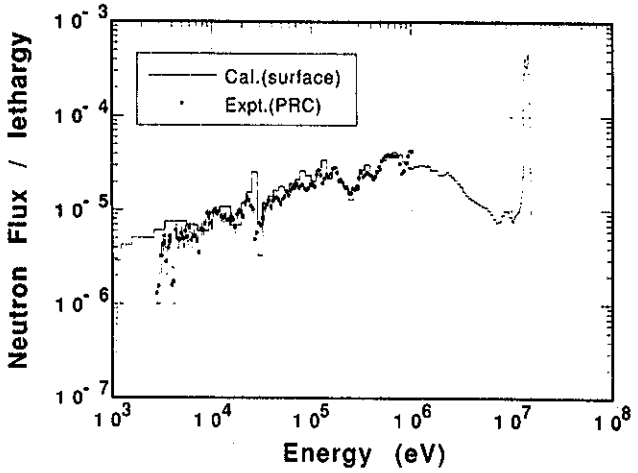

Fig. 19. Neutron spectrum at the front surface of the test assembly, Phase IIIA.

DOT3.5 and MORSE-DD calculations (JAERI) and along the axis of drawer B. In phase IIIC, the results shown are based on the Monte Carlo calculations with JENDL-3 (J3) and JENDL-3PR2 (PR2) data where it is clear that the J3 data give values of C/E closer to unity than the PR2 data. The high-energy component of the spectrum is under predicted in all phases, and the DOT results are larger than those of the Monte Carlo, particularly at front locations in the assembly, as was discussed earlier.

IV.C. Tritium Production Rate

IV.C.1. Tritium Production Rate from ^7Li (T_7)

The profiles of local T_7 inside drawer B in the radial direction, as measured by NE213 (on-line, stepwise

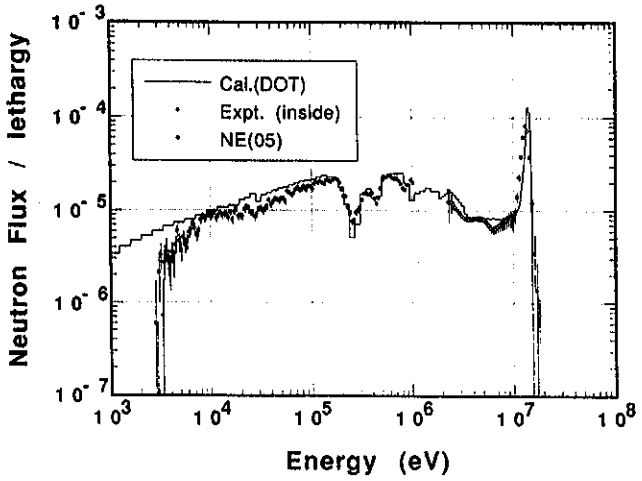

Fig. 20. Neutron spectrum inside the test assembly, Phase IIIA.

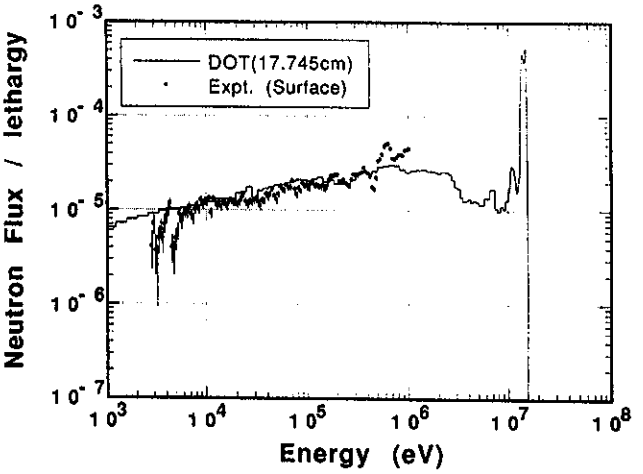

Fig. 21. Neutron spectrum at the front surface of the test assembly, Phase IIIB.

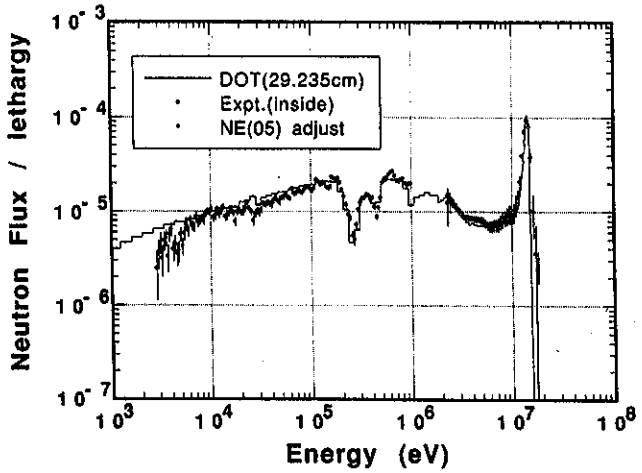

Fig. 22. Neutron spectrum inside the test assembly, Phase IIIB.

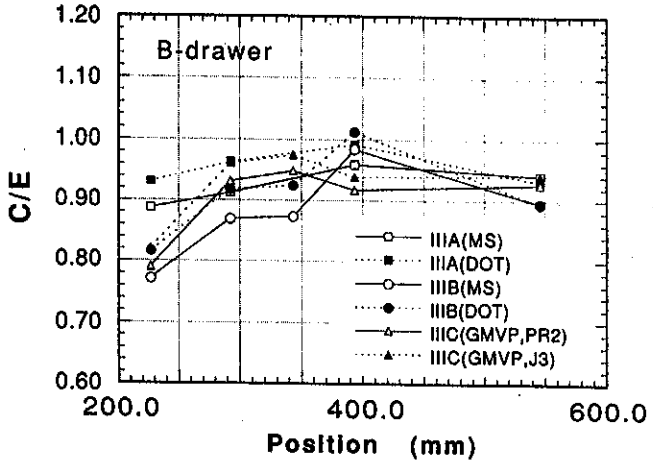

Fig. 23. The C/E value for the integrated spectrum above 1 MeV in Phases IIIA, IIIB, and IIIC.

operation mode), are shown in Figs. 24a, 24b, and 24c for Phases IIIA, IIIB, and IIIC, respectively, along with the calculated values obtained by various codes and databases. The experimental errors with the NE213 method are within the size of the markers used in the graphs. The calculated values are in good agreement with the measured ones. Generally, the steepness of the T_7 profile is more pronounced in Phase III as compared to other phases performed with the 14-MeV point source since in the latter case, the assembly is located at a larger distance from the source [~78 cm in Phase II (Ref. 5), ~248 cm in Phase I (Ref. 2)] and therefore the inverse of the square distance effect is dominant in Phase III for threshold reactions such as T_7.

The impact of the inclusion of the armor layer on T_7 can be seen from Fig. 25 where the ratio of local T7 in Phase IIIB to those in Phase IIIA are depicted and are estimated from the experimental (NE213) and calculated results. The decrease in local T_7 is ~8 to 10% as obtained from the experimental data; however, the predicted decrease is larger when calculated by all codes and databases. The change in the neutron spectrum behind the armor layer, as measurements indicate, is such that more neutrons are moderated to the energy range below a few keV [where $^6Li(n,\alpha)t$ cross section is large] and above a few MeV [where the threshold of the $^7Li(n,n')\alpha t$ reaction lies] and fewer neutrons are moderated to the energy range a few keV to a few MeV. On the other hand, the spectrum predicted with the carbon data is such that fewer neutrons are moderated to the energy range below a few keV and above a few MeV, and more neutrons are moderated in the energy range a few keV to a few MeV. This led to the larger ratios (above 0.9) obtained from measurements compared to those obtained from calculations, as shown in Fig. 25. Based on JAERI's results from the Monte Carlo codes (MORSE-DD, GMVP) and the discrete ordinates DOT3.5 code, the decrease in local T_7 is ~12 to 14% while the largest decrease (~18%) is predicted by the DOT5.1 code. In Fig. 25 and all subsequent figures, the transport and response calculation of MORSE-DD are based on JENDL-3PR2 data while the transport calculation of GMVP is based on JENDL-3 data. In the

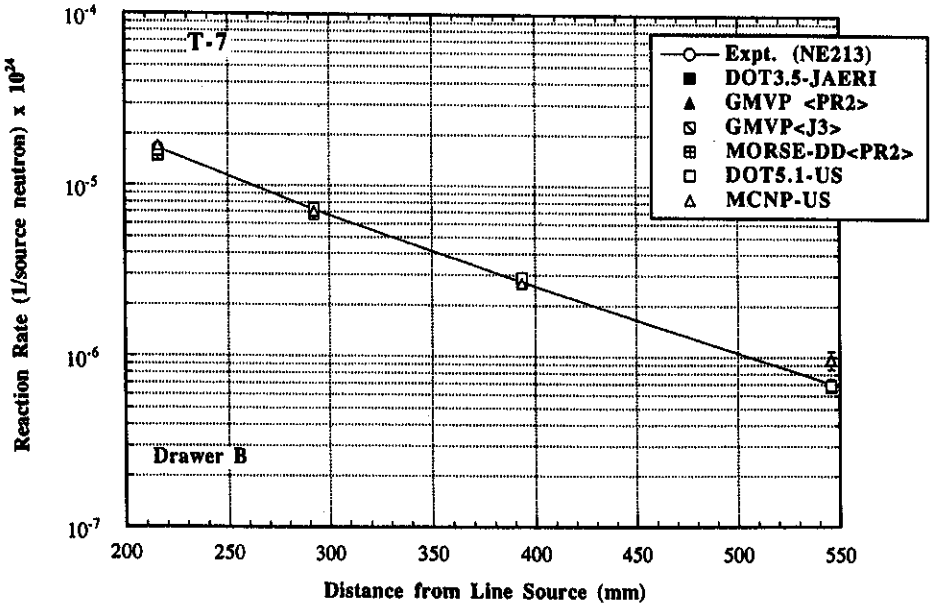

Fig. 24a. Profiles of TPR from ^7Li along drawer B, Phase IIIA.

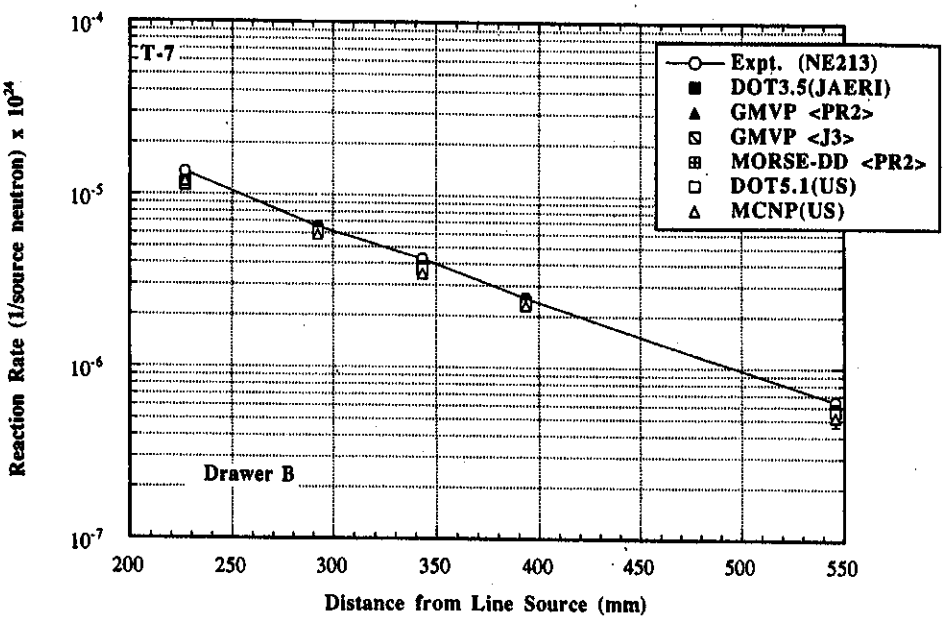

Fig. 24b. Profiles of TPR from ^7Li along drawer B, Phase IIIB.

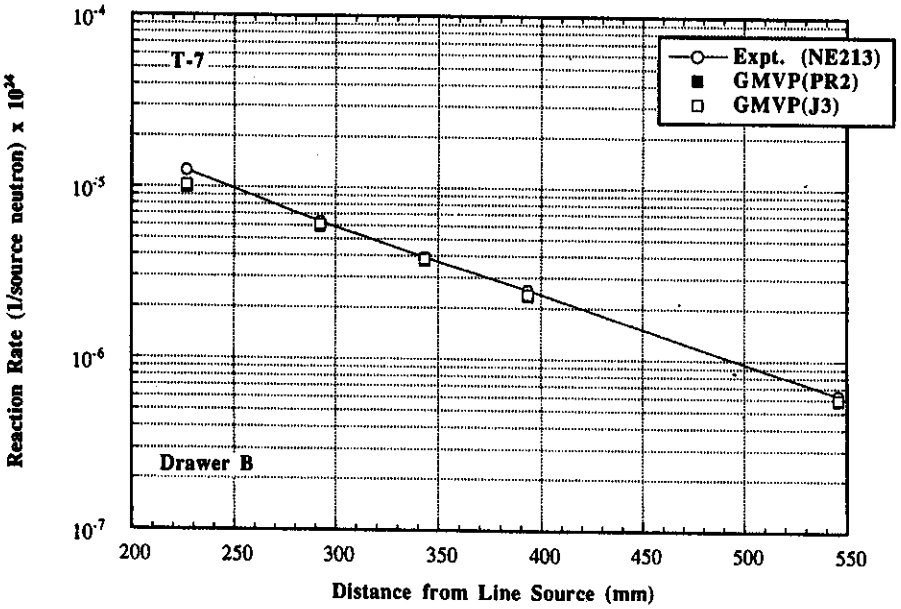

Fig. 24c. Profiles of TPR from ^7Li along drawer B, Phase IIIC.

later case, the response (e.g., T_7, T_6 . . .) has been calculated from JENDL-3PR2 [denoted GMVP (PR2)] and from JENDL-3 [denoted GMVP(J3)]. The decrease in local T_7 has also been measured in the other drawers (A & C) and in the axial Z direction at a radial distance of 279 mm and 380 mm from the line source where it has been shown that the decrease in local T_7 is more pronounced at locations toward the front and back ends of the assembly.[17]

The effect of the large opening on T_7 profiles in drawer B (facing the opening on the other no-hole side) is shown in Fig. 26 where the ratio of local T_7 in Phase IIIC to those in Phase IIIB is given. The measurements show a decrease at all locations due to the

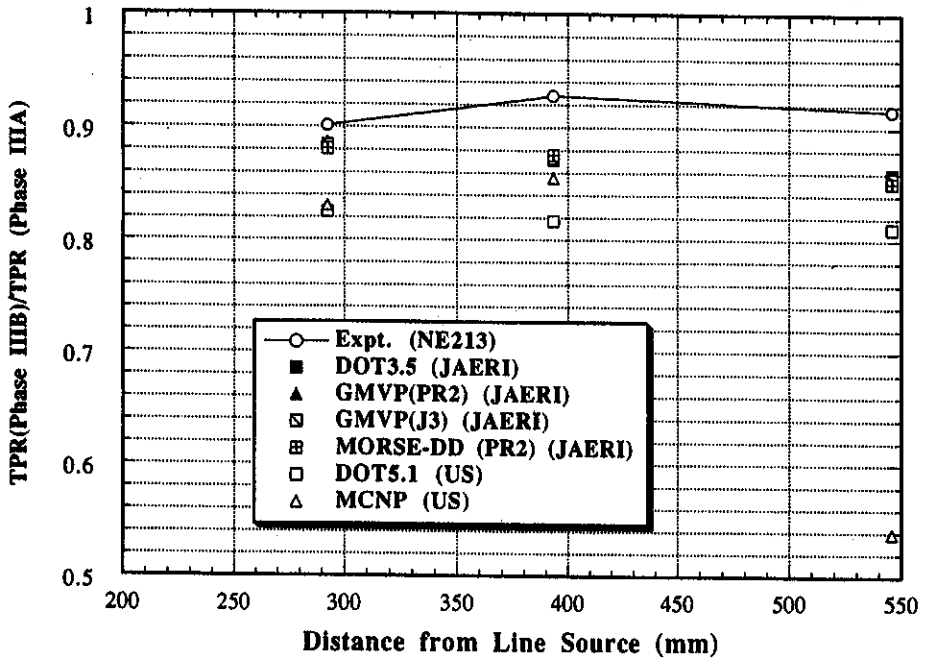

Fig. 25. Ratio of local TPR from ^7Li (T_7) in drawer B of Phase IIIB to corresponding values in Phase IIIA (NE213 measurements).

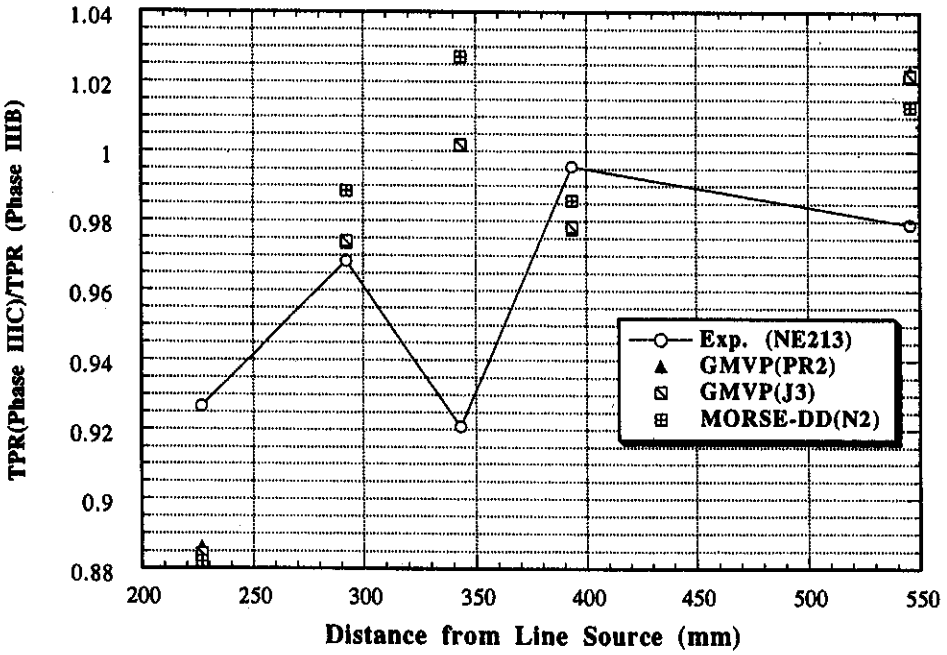

Fig. 26. Ratio of local TPR from ^7Li (T_7) in drawer B of Phase IIIC to corresponding values in Phase IIIB (NE213 measurements).

existence of the opening by values that vary between 0.5 to 8%. Although the calculations show a decrease in local T_7 at a radial direction of 292.4 mm and 393.4 mm by ~1 to 2.5%, the ratios are larger than unity at other locations by ~1.5 to 3%.

Table II gives the numerical values of measurements and calculations of local T_7 (units of T/atom·source neutron) measured by NE213 in the three phases, and they are consistent with the graphical values depicted in Figs. 24. The C/E curves are shown in

TABLE II

Calculational and Experimental Values for Tritium Production Rate from ^7Li (T_7) Measured by NE213 Detectors in Drawer B of Phase IIIA, Phase IIIB, and Phase IIIC

Position (mm)	Experiment	Error	DOT5.1 (U.S.)	DOT3.5 (JAERI)	MCNP (U.S.)	Error (%)	MORSE-DD (JAERI)	GMVP (JAERI) PR 2	Error (%)	GMVP (JAERI) J3	Error (%)
Phase IIIA											
2.16000e+02[a]	1.65900e−05	6.1027	1.58700e−05	1.57700e−05	1.70200e−05	2.900	1.50260e−05	1.47360e−05	0.3500	1.54490e−05	0.3500
2.26700e+02											
2.92400e+02	7.25740e−06	6.0086	7.36300e−06	7.15380e−06	7.04400e−06	4.500	6.78100e−06	6.84070e−06	0.5300	7.07000e−06	0.5300
3.43400e+02		6.0121									
3.93400e+02	2.74680e−06	5.9994	2.90500e−06	2.78860e−06	2.68800e−06	7.100	2.69700e−06	2.72370e−06	0.8300	2.79170e−06	0.8300
5.45800e+02	7.06280e−07		6.89900e−07	6.73180e−07	9.67400e−07	12.000	6.80480e−07	6.70210e−07	0.1510	6.81820e−07	0.1510
Phase IIIB											
2.26700e+02	1.35510e−05	6.1650	1.13600e−05	1.19140e−05	1.19100e−05	2.700	1.12620e−05	1.12100e−05	0.4200	1.16570e−05	0.4200
2.92400e+02	6.54050e−06	6.1509	6.07300e−06	6.30170e−06	5.84900e−06	4.300	5.97390e−06	6.06560e−06	0.5500	6.25160e−06	0.5500
3.43400e+02	4.28380e−06	6.1609	3.75800e−06	3.86020e−06	3.50000e−06	4.000	3.64640e−06	3.73940e−06	0.7000	3.83870e−06	0.6900
3.93400e+02	2.54970e−06	6.0722	2.37300e−06	2.43060e−06	2.30000e−06	7.200	2.36290e−06	2.38250e−06	0.8700	2.43700e−06	0.8600
5.45800e+02	6.46830e−07	5.9812	5.59600e−07	5.78600e−07	5.21100e−07	1.200	5.79820e−07	5.74100e−07	0.1610	5.83730e−07	0.1610
Phase IIIC											
2.26700e+02	1.25580e−05	5.91461						9.93270e−06	0.64	1.0309e−05	0.64
2.92400e+02	6.33440e−06	6.4955						5.90530e−06	0.71	6.0900e−06	0.71
3.43400e+02	3.94500e−06	6.2769						3.74530e−06	0.87	3.8457e−06	0.87
3.93400e+02	2.53890e−06	6.0984						2.32920e−06	1.08	2.3840e−06	1.07
5.45800e+02	6.33420e−07	6.0178						5.87350e−07	1.90	5.9664e−07	1.90

[a]Read as 2.16000×10^2.

Figs. 27, 28, and 29 for Phases IIIA, IIIB, and IIIC, respectively. In Phase IIIA, the C/E values lie between 0.9 and 1.05 (except for the MCNP value of 1.38 at R = 545.8 mm where the statistical error is ~12%, see Table II), indicating that the prediction uncertainty in local T_7 is about −10% to +5% in Phase IIIA, but on the average, the C/E values are lower than unity by ~5%. Since the predicted decrease in local T_7 upon the inclusion of the armor layer is larger than the corresponding decrease detected by NE213 (see Fig. 25), the corresponding C/E curves in Phase IIIB (see Fig. 28) are lower in absolute values than those of Phase IIIA. In Phase IIIB, all the C/E values are lower than unity by an average value of ~10 to 15%. The C/E curves in Phase IIIC are shown in Fig. 29, where some oscillating trend in these curves can be seen due to the same trend found in the ratios of local T_7 in Phase IIIC relative to Phase IIIB values. At all locations, the C/E values are still lower than unity as in Phase IIIB. It should be noticed in Figs. 27, 28, and 29 that the errors in the C/E values are overlapping at most locations. These errors include both the calculational and experimental errors. The C/E values obtained by GMVP with JENDL-3 data are closer to unity than those obtained with the response calculated from the J3/PR2 database [the calculated T_7 with GMVP/J3 are larger than that with GMVP/PR2 (see Figs. 24 and 27, 28, and 29)].

IV.C.2. Tritium Production Rate from ^6Li (T_6)

The calculated and measured profiles of local T_6 in drawer B are shown in Figs. 30a, 30b, and 30c, for Phases IIIA, IIIB, and IIIC, respectively. The measured data sets of the Li-glass detectors (on-line, stepwise operation mode) are shown with their associated errors. The calculated T_6 by various codes and databases, along with the associated statistical errors in the Monte Carlo calculations, are also given in Fig. 30 where good

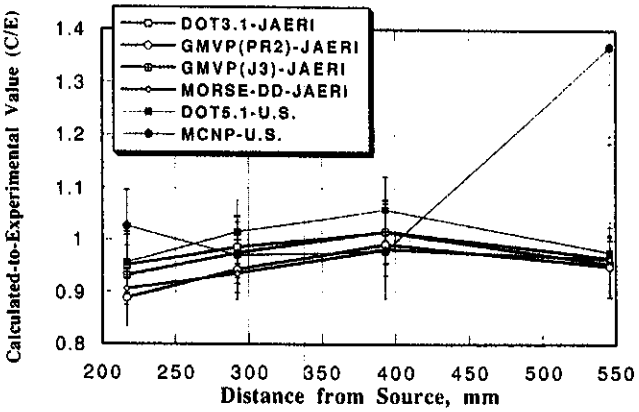

Fig. 27. The C/E values of tritium production rate from $^7Li(T_7)$ in the radial direction along drawer B of Phase IIIA (NE213 measurements).

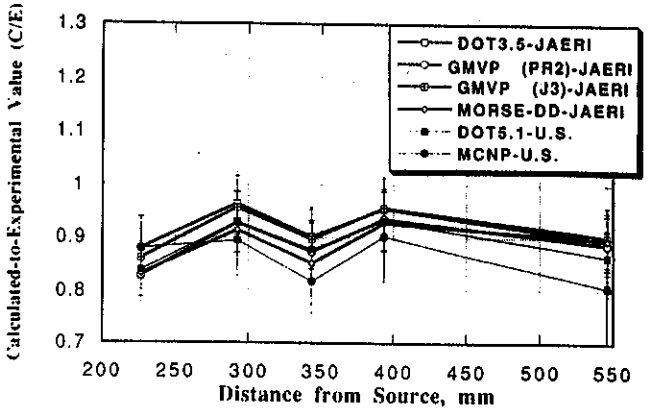

Fig. 28. The C/E values of tritium production rate from $^7Li(T_7)$ in the radial direction along drawer B of Phase IIIB (NE213 measurements).

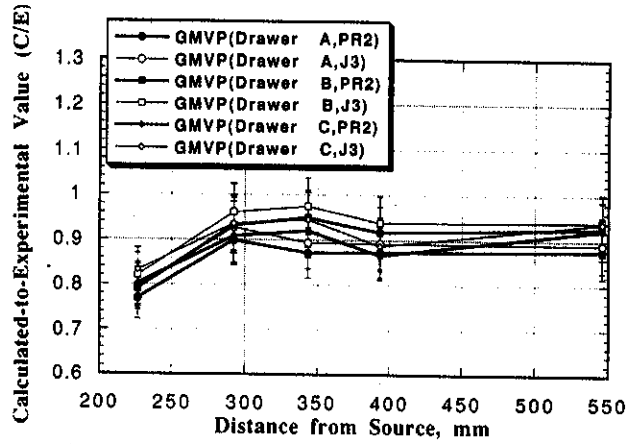

Fig. 29. The C/E values of tritium production rate from $^7Li(T_7)$ in the radial direction along drawer B of Phase IIIC (NE213 measurements).

agreement with the Li-glass measurements can be observed. The profiles themselves are almost flat in the radial direction, as opposed to steeper profiles found in the other 14-MeV point source experiments.[2,5] This feature is attributed to the simulated line source where every spatial point on the 2-m length line source contributes to the nonthreshold $^6Li(n,\alpha)t$ reactions, even at deeper locations inside the Li_2O zone, contrary to the T_7 case, which is dominated by high energy neutrons. Consequently, the T_6 profiles in the Z direction (see Ref. 17), which assume a cosine-shape, are wider than those of T_7 in the Z direction. These trends have also been demonstrated through the preanalysis of the line-source experiments.[13]

As mentioned earlier, the change in the spectrum behind the armor layer, as measurements indicate, is such that more neutrons are moderated to the energy

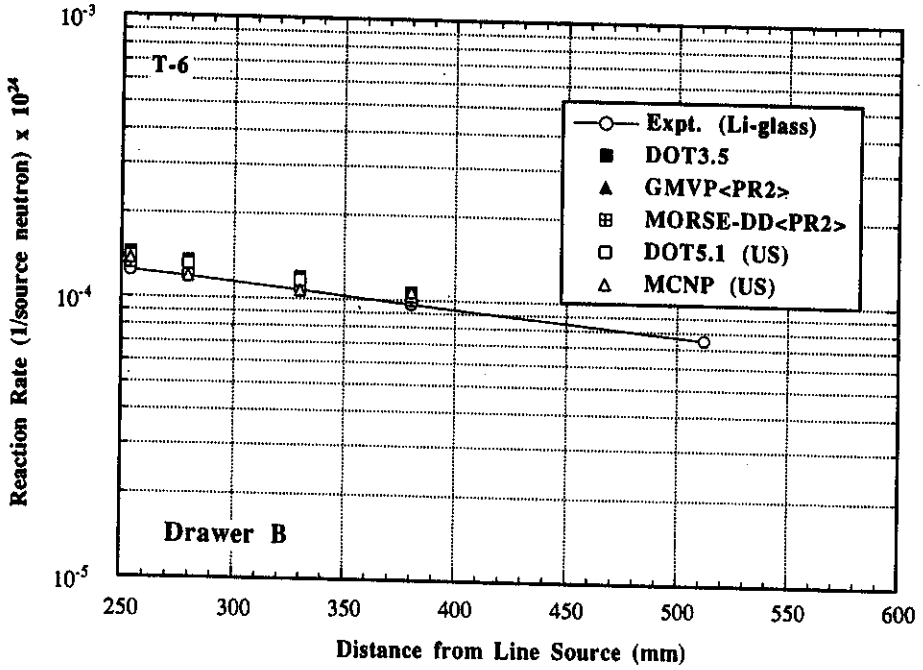

Fig. 30a. Profiles of TPR from ^6Li along drawer B, Phase IIIA.

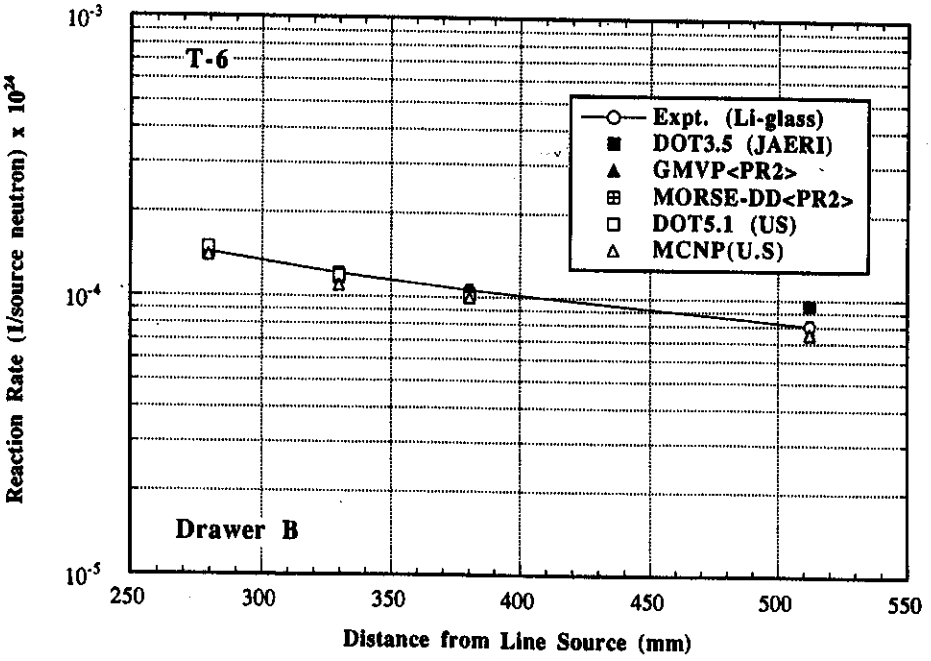

Fig. 30b. Profiles of TPR from ^6Li along drawer B, Phase IIIB.

range below a few keV [where the $^6Li(n,\alpha)t$ cross-section is large] and above a few MeV, and fewer neutrons are moderated to the energy range few keV–few MeV. This trend is reversed, as obtained from calculations. Consequently, measurements indicate more increase in local T_6 upon the inclusion of the armor layer compared to calculations as shown in Fig. 31. The measured increase is ~20% (at front locations) to ~10%

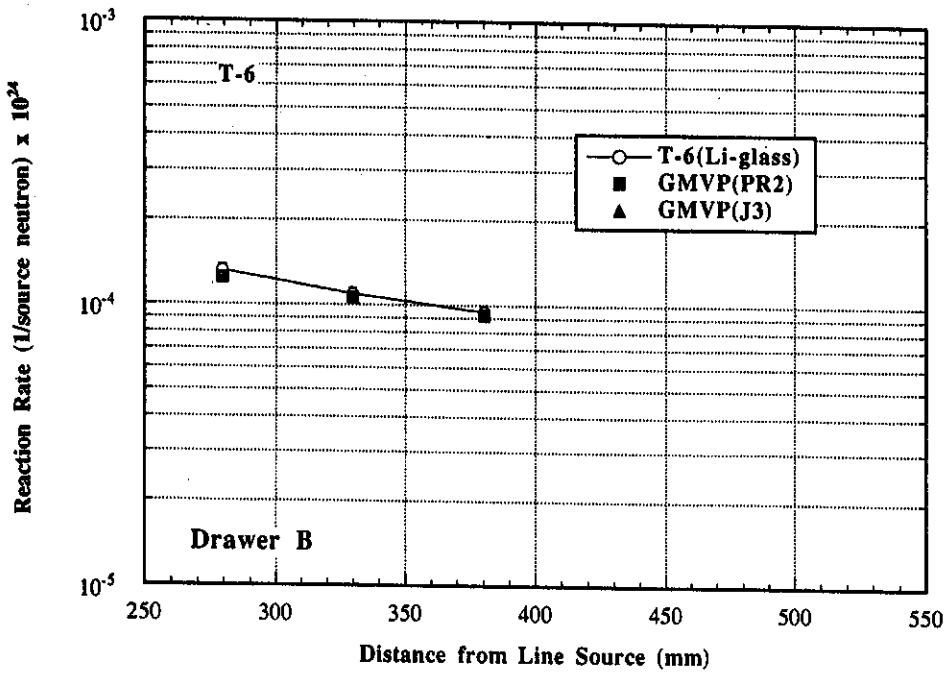

Fig. 30c. Profiles of TPR from ^6Li along drawer B, Phase IIIC.

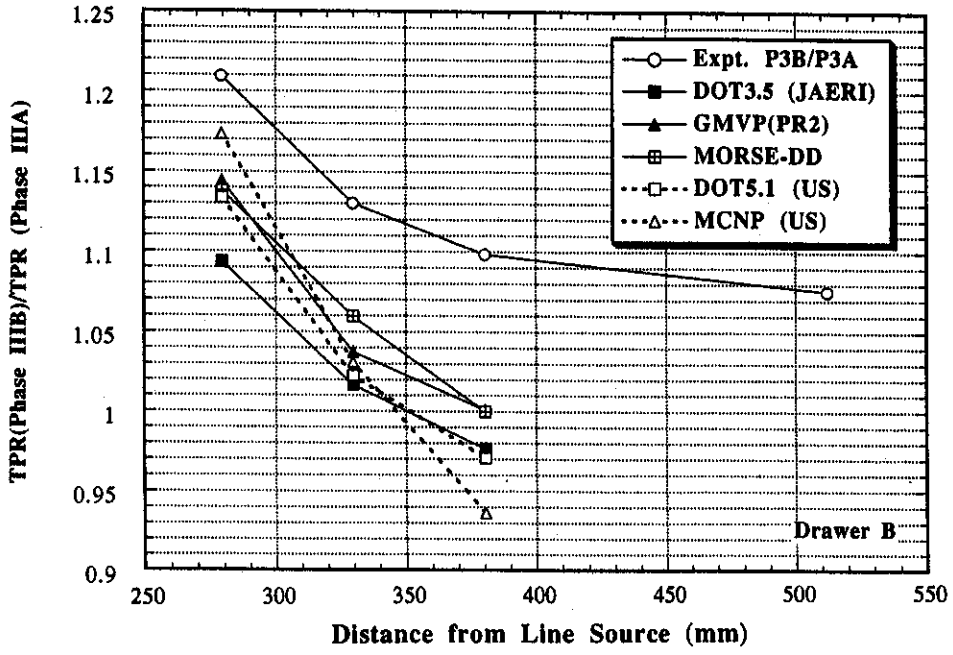

Fig. 31. Ratio of local TPR from ^6Li (T_6) in drawer B of Phase IIIB to corresponding values in Phase IIIA (measurements: Li-glass).

(at back locations). The predicted increase is ~14% (with GMVP, MORSE-DD, DOT5.1), ~17% (MCNP), and ~9% (DOT3.5) at the very front locations. However, at a distance greater than ~330 mm from the line source (~102-mm depth inside the Li_2O zone), the results based on MCNP, DOT3.5, and DOT5.1 showed a decrease in local T_6, contrary to the measured trend. The effect of the opening in Phase IIIC on local T_6 in

drawer B is shown in Fig. 32. The Li-glass measured data show a decrease of ~8% at front locations and ~11% at back locations. The corresponding decrease predicted with GMVP code is ~13% and 9%. This decrease is due to the decrease in the reflected low-energy neutrons incident on the no-hole side resulting from the presence of the opening. It was shown that such a decrease is confined to a width in the axial direction corresponding to the width of the opening[17] (42.5 cm). It should be noted that the predicted decrease in T_6 at front locations (~13%) is comparable to the predicted increase (~14%) resulting from the inclusion of the armor layer, rendering local T_6 to have values similar to those found in Phase IIIA.

Table III shows the numerical data of the measurements and calculations for local T_6 in drawer B as obtained in the three phases. The relevant C/E curves are shown in Figs. 33, 34, and 35. In Phase IIIA, the C/E values are generally larger than unity by 5 to 15% and the curves have a flat shape (i.e., no spatial dependence), except for the results based on MCNP calculations. Since the predicted increase in local T_6 when the armor layer is added is less pronounced than those obtained from measurements, the overestimation in T_6 in phase IIIA is compensated for in Phase IIIB, leading to C/E values that are on the average lower than unity by ~5% inside the Li_2O zone, as shown in Fig. 34 (MORSE-DD and DOT3.5 results are larger than measurements inside the Li_2CO_3 layer). The C/E curves in Phase IIIC are also flat and the calculated values by the GMVP code are lower than the measured ones by ~5%, as shown in Fig. 35. Notice that the results based on the JENDL-3 data are better than those based on JENDL-3PR2. Also, the errors in the C/E values are overlapping at almost all locations.

V. THE PREDICTION UNCERTAINTY IN LOCAL AND LINE-INTEGRATED TPR

Table IV summarizes the overall prediction uncertainty in local TPR from ^6Li and ^7Li in the three phases of the line source experiments. For a given phase, the prediction uncertainty is the average of the quantity $[(C/E) - 1] \times 100$ estimated at all locations where measured data were taken inside the Li_2O zone. These average values are based on both the U.S. and JAERI results. As can be seen, local T_7 is underestimated by 5 to 15% based on the NE213 results. Local T_6 measured by Li-glass detectors, on the other hand, is overestimated in Phase IIIA by ~5 to 15% while it is underestimated in Phases IIIB and IIIC by ~5%.

More rigorous treatments were made to quantify the prediction uncertainty in local and line-integrated TPR from ^6Li and ^7Li in all the experiments performed under the U.S. DOE/JAERI collaborative program on fusion blanket neutronics. For more details on the methodology followed to quantify these prediction uncertainties, the reader is referred to Refs. 29 through 32. Briefly, the best fitting curve (by the least-squares method) for the measured data is integrated in the radial direction, and uncertainty (error) in the

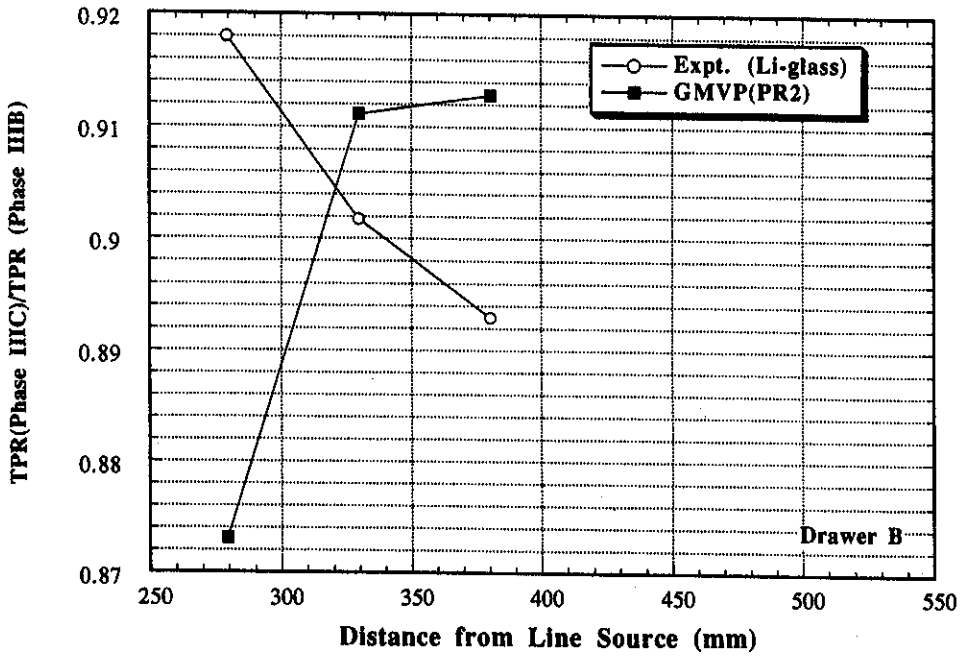

Fig. 32. Ratio of local TPR from ^6Li (T_6) in drawer B of Phase IIIC to corresponding values in Phase IIIB (measurements: Li-glass).

TABLE III

Calculational and Experimental Values for Tritium Production Rate from ^6Li (T_6) Measured by Li-Glass Detectors in Drawer B of Phases IIIA, IIIB, and IIIC

Position (mm)	Experiment	Error (%)	DOT5.1 (U.S.)	DOT3.5 (JAERI)	MCNP (U.S.)	Error (%)	MORSE-DD (JAERI)	GMVP (JAERI)	Error (%)
Phase IIIA									
254.00	1.24350e−04[a]	4.911	1.39900e−04	1.44190e−04	1.37000e−04	5.400	1.32160e−04	1.32400e−04	0.2900
279.40	1.18750e−04	4.499	1.31800e−04	1.35170e−04	1.19300e−04	4.400	1.24590e−04	1.25040e−04	0.2900
329.80	1.07370e−04	4.307	1.16300e−04	1.19130e−04	1.06700e−04	4.200	1.10500e−04	1.12270e−04	0.3000
380.40	9.67180e−05	4.326	1.03100e−04	1.06000e−04	1.06600e−04	5.800	1.00090e−04	1.01010e−04	0.3300
512.20	7.49420e−05	4.256							
Phase IIIB									
2.79400e+02	1.43630e−04	5.033	1.49400e−04	1.47820e−04	1.40000e−04	5.000	1.41790e−04	1.43050e−04	0.3300
3.29800e+02	1.21340e−04	4.721	1.18900e−04	1.21130e−04	1.10000e−04	4.500	1.17100e−04	1.16500e−04	0.3100
3.80400e+02	1.06250e−04	4.564	1.00100e−04	1.03520e−04	9.98100e−04	4.200	1.00100e−04	1.01100e−04	0.3300
5.12200e+02	8.06150e−05	4.515		9.55690e−05	7.51000e−05	5.000	9.38250e−05	7.54950e−05	0.4200
Phase IIIC									
2.79400e+02	0.00013185	4.9360						0.00012448	0.38000
3.29800e+02	0.00010942	4.7300						0.00010580	0.39000
3.80400e+02	9.4882e−05	4.7570						9.1957e−05	0.41000

[a]Read as 1.24350×10^{-4}.

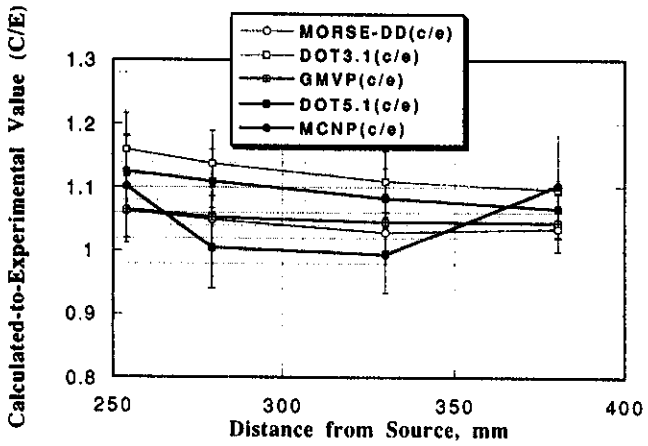

Fig. 33. The C/E values of tritium production rate from $^6Li(T_6)$ in the radial direction along drawer B of Phase IIIA (Li-glass measurements).

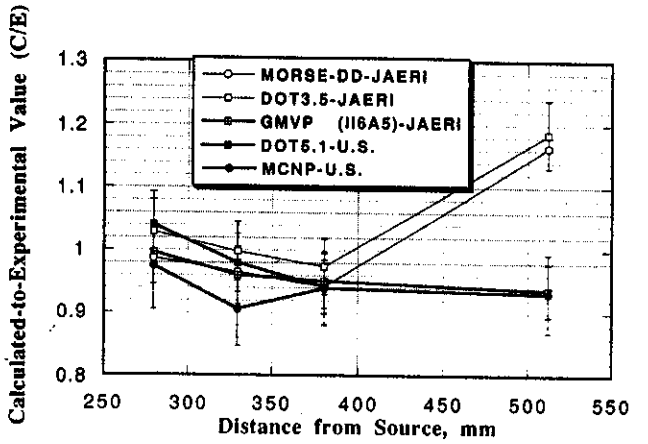

Fig. 34. The C/E values of tritium production rate from $^6Li(T_6)$ in the radial direction along drawer B of Phase IIIB (Li-glass measurements).

integrated value, E_{int}, is estimated from the uncertainties in the fitting coefficients which account for the uncertainty in the measured data. The same procedures are applied to the calculated data at the locations where measurements are taken. An estimate is then made to the value $[(C/E)_{int} - 1] \times 100$ and the associated relative standard deviation, σ_i. These prediction uncertainties and associated errors are listed in Table V for the line-integrated T_6 and T_7 based on Li-glass and NE213 measurements.

By examining Tables IV and V, the prediction uncertainty in line-integrated T_6 is similar to the average prediction uncertainty in local values evaluated in drawer B; e.g., overprediction in Phase IIIA by 5 to 15%, and generally underprediction in Phases IIIB and IIIC by ~2 to 6%. As for the line-integrated T_7, it is underpredicted in all the drawers of Phase IIIB and IIIC by 8 to 15% (as opposed to the underprediction of 10 to 15% in the local values, see Table IV). Underprediction by ~6% in Phase IIIA can also be seen from Table V, particularly in the GMVP case, which is similar to the underprediction (~5%) in local values. The standard deviation around these mean values is ~2 to 6%.

It should be noted that the observed differences between the results of the U.S. and JAERI cited here are attributed to the differences in nuclear data libraries used, their group structure, and the input specification of the calculational methods applied. This includes, for

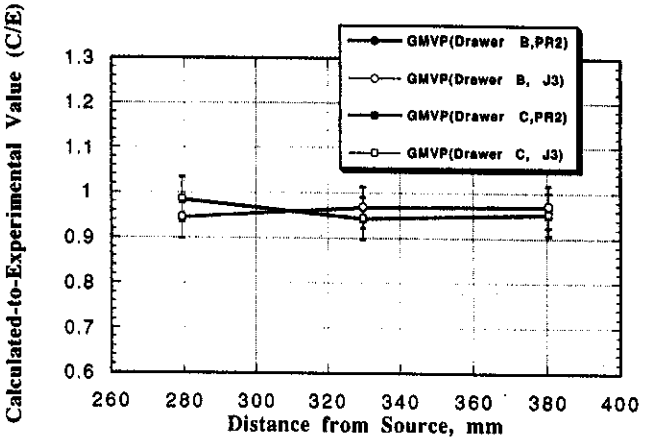

Fig. 35. The C/E values of tritium production rate from $^6Li(T_6)$ in the radial direction along drawer B of Phase IIIC (Li-glass measurements).

TABLE IV

Average Values of the Prediction Uncertainty, $[(C/E) - 1] \times 100$, in Local Tritium Production Rate from ^6Li and ^7Li

Tritium Production Rate from ^6Li (T_6)	
Phase	Li-Glass Method (%)
IIIA	5 to 15
IIIB	−5
IIIC	−5
Tritium Production Rate from ^7Li (T_7)	
Phase	NE213 Method (%)
IIIA	−5
IIIB	−10 to −15
IIIC	−10

TABLE V

The Prediction Uncertainty, [(C/E) − 1] × 100, of the Line-Integrated Tritium Production Rate from ^6Li (T_6) and ^7Li (T_7)*†

Phase	U.S.		JAERI			
	DOT5.1	MCNP	DOT3.5	MORSE-DD	GMVP (PR2)	GMVP (J3)
Line-Integrated Tritium Production Rate from ^6Li (T_6)						
Phase IIIA						
Drawer B	8.8 (±3.1)[a]	9.4 (±5.0)	11.9 (±3.1)	4.5 (±3.1)	5.2 (±3.1)	
Draser C	10.7 (±4.4)	3.7 (±6.9)	12.5 (±4.4)	4.0 (±4.5)	5.3 (±4.5)	
Phase IIIB						
Drawer B	−1.9 (±2.8)	−6.6 (±3.9)	−0.3 (±2.8)	−3.8 (±2.8)	−3.4 (±2.8)	
Drawer C	3.9 (±3.5)	−4.1 (±4.0)	3.3 (±3.5)	−1.7 (±3.5)	−0.3 (±2.9)	
Phase IIIC						
Drawer B					−4.7 (±4.9)	−4.4 (±4.9)
Drawer C					−2.4 (±4.9)	−2.0 (±4.9)
Line-Integrated Tritium Production Rate from ^7Li (T_7)						
Phase IIIA						
Drawer A	−0.4 (±3.8)	0.2 (±5.0)	−2.9 (±3.8)		−6.7 (±3.8)	−3.5 (±3.8)
Drawer B	1.3 (±2.1)	−1.5 (±3.7)	−1.4 (±3.8)		−5.6 (±3.8)	−2.4 (±3.8)
Drawer C	2.7 (±3.8)	1.7 (±5.1)	−2.3 (±3.9)		−5.8 (±3.9)	−5.8 (±3.9)
Phase IIIB						
Drawer A	−8.9 (±1.8)	−9.3 (±3.9)	−5.1 (±3.2)	−7.7 (±3.2)	−9.7 (±3.2)	−6.9 (±3.2)
Drawer B	−10.8 (±3.2)	−11.4 (±3.8)	−7.6 (±3.2)	−11.9 (±3.2)	−11.2 (±3.2)	−8.4 (±3.2)
Drawer C	−8.6 (±3.2)	−11.1 (±3.8)	−6.5 (±3.2)	−10.8 (±3.2)	−10.5 (±3.2)	−7.6 (±3.2)
Phase IIIC						
Drawer A					−15.3 (±3.1)	−12.8 (±3.1)
Drawer B					−11.4 (±3.2)	−8.7 (±3.2)
Drawer C					−13.2 (±3.1)	−10.6 (±3.1)

*From Ref. 29.
†T_6: Li-glass measurements, T_7: NE213 measurements.
[a]Relative standard deviation, σ_i, in the $(C/E)_{int}$ value; it includes the calculational and experimental errors in the Monte Carlo cases and only the experimental errors in the discrete ordinates cases.

example, the level of the discretization in the discrete ordinates method (e.g., S_nP_l approximation) and the number of histories in the Monte Carlo calculation. The impact of these specifications on the calculated results was investigated and discussed in Refs. 33 and 34.

VI. SUMMARY

Integral fusion neutronics experiments with a simulated line source have been performed to better simulate the incident neutron source conditions found in tokamak reactors. The characteristics of the simulated line source were examined by various flux and foil activation measurements (with and without the annular test assembly in place) and comparisons were made with calculations using various codes and nuclear data. The agreement with foil activation measurements is within 5 to 10% (bare line source) and within 10 to 20% (with the annular assembly surrounding the line source). The annular blanket experiments were performed in three phases. In Phase IIIA, the reference blanket consisted of a 1.5-cm-thick first wall followed by the Li_2O and the Li_2CO_3 zones. Phase IIIB is dedicated to studying the impact of the inclusion of 2.45-cm-thick armor (carbon) layer on blanket characteristics, while Phase IIIC focused on studying these characteristics in the presence of a large opening at one side of the annular assembly. Foil activation measurements inside the assembly indicated good agreement with calculations within 5% for some reaction rates and within 10% for some others. In-system spectrum is reasonably predicted except that the high-energy component is underpredicted in all phases and the discrete ordinates results are larger than

the results based on the Monte Carlo calculations. This was also reflected on the several reaction rates measured inside the assembly where the C/E values based on DOT calculations were larger than those based on MCNP, MORSE-DD, and GMVP Monte Carlo codes.

The armor layer tends to decrease local TPR from ^7Li (T_7) and to increase local TPR from ^6Li (T_6). The decrease in T_7 measured by the NE213 detectors is less pronounced than the calculated values, while the increase in T_6 detected by the Li-glass method is more pronounced than the predicted values. The change in the spectrum behind the armor layer, as measurements indicate, is such that more neutrons are moderated to the energy range below a few keV [where $^6Li(n,\alpha)t$ cross section is large] and above a few MeV and fewer neutrons are moderated to the energy range a few keV to a few MeV. This trend is reversed, as obtained from calculations. Additionally, the increase in T_6 is detected at all locations inside the Li_2O zone, while calculations showed that a decrease in local T_6 could occur at back locations. The effect of the large opening of Phase IIIC on local T_7 is such that reduction in their values occurs at front locations of the breeding zone facing the opening. Local T_6 also decreases with an amount comparable to the increase achieved due to the inclusion of the armor layer, rendering local T_6 to have values similar to those found in Phase IIIA.

The average values of the prediction uncertainties in local as well as line-integrated TPR (which has closer similarity to the tritium breeding ratio, TBR, in a blanket) have been calculated based on results from all codes/databases, along with the associated errors arising from the statistical errors in the calculations and the evaluated experimental errors. The prediction uncertainty in the line-integrated T_6 is similar to the average prediction uncertainty in local values, which are overpredicted in Phase IIIA by 5 to 15%, and generally underpredicted in Phases IIIB and IIIC by ~2 to 6%. As for the line-integrated T_7, it is underpredicted in all the drawers of Phases IIIB and IIIC by 8 to 15%. Underprediction in the integrated T_7 by ~6% was also found in Phase IIIA, which is similar to the underprediction (~5%) in local values. The standard deviation around the mean values of the prediction uncertainties is ~2 to 6%. These estimates are based on the Li-glass measurements of T_6 and NE213 measurements of T_7. Generally, the results based on Monte Carlo calculations are closer to the experimental values than those based on the discrete ordinates method. The results based on DOT calculations are, on the average, larger than the results obtained from the Monte Carlo calculations.

ACKNOWLEDGMENT

The U.S. effort in the reported joint work has been conducted under the U.S. Department of Energy grant DOE-FG03-88ER52150.

REFERENCES

1. T. NAKAMURA and M. A. ABDOU, "Summary of Recent Results from the JAERI/US Fusion Neutronics Phase I Experiment," *Fusion Technol.*, **10**, 541 (1986).

2. M. Z. YOUSSEF, C. GUNG, M. NAKAGAWA, T. MORI, K. KOSAKO, and T. NAKAMURA, "Analyses and Intercomparison for Phase I Fusion Integral Experiments at the FNS Facility," *Fusion Technol.*, **10**, 549 (1986).

3. M. Z. YOUSSEF et al., "Phase I Fusion Integral Experiments, Vol. II: Analysis," UCLA-ENG-88-15, University of California, Los Angeles (Sep. 1988); see also JAERI-M-88-177, Japan Atomic Energy Research Institute (Aug. 1988).

4. M. NAKAGAWA et al., "Analysis of Neutronics Parameters Measured in Phase II Experiments of JAERI/U.S. Collaborative Program on Breeder Neutronics, Part I: Source Characteristics and Reaction Rate Distribution," *Fusion Eng. Des.*, **9**, 315 (1989).

5. Y. OYAMA, K. TSUDA, S. YAMAGUCHI, Y. IKEDA, C. KONNO, H. MAEKAWA, and T. NAKAMURA, "Phase II Experimental Results of JAERI/USDOE Collaborative Program on Fusion Blanket Neutronics Experiments," *Fusion Eng. Des.*, **9**, 309 (1989).

6. M. Z. YOUSSEF, Y. WATANABE, C. Y. GUNG, M. NAKAGAWA, T. MORI, and K. KOSAKO, "Analysis of Neutronics Parameters Measured in Phase II Experiments of the JAERI/U.S. Collaborative Program on Fusion Blanket Neutronics, Part II: Tritium Production and In-System Spectrum," *Fusion Eng. Des.*, **9**, 323 (1989).

7. Y. OYAMA et al., "Phase IIB Experiments of JAERI/USDOE Collaborative Program on Fusion Blanket Neutronics," *Fusion Technol.*, **15**, 1293 (1989).

8. M. Z. YOUSSEF et al., "Comparative Analysis for Phase IIA and IIB Experiments of the U.S./JAERI Collaborative Program on Fusion Blanket Neutronics," *Fusion Technol.*, **15**, 1299 (1989).

9. Y. IKEDA, C. KONNO, Y. OYAMA, K. OISHI, and T. NAKAMURA, "Determination of Neutron Spectrum in D-T Fusion Field by Foil Activation Technique," *Fusion Technol.*, **15**, 1287 (1989).

10. M. Z. YOUSSEF, M. A. ABDOU, Y. WATANABE, and P. M. SONG, "The U.S./JAERI Collaborative Program on Fusion Neutronics; Phase IIA and IIB Fusion Integral Experiments, The U.S. Analysis," UCLA-ENG-90-14, University of California at Los Angeles (Dec. 1989).

11. M. NAKAGAWA, T. MORI, K. KOSAKO, Y. OYAMA, and T. NAKAMURA, "JAERI/U.S. Collaborative Program on Fusion Blanket Neutronics, Analysis of Phase IIA and IIB Experiments," JAERI-M-89-154, Japan Atomic Energy Research Institute (Oct. 1989).

12. M. Z. YOUSSEF et al., "Analysis for Heterogeneous Blankets and Comparison to Measurements: Phase IIC Experiments of the USDOE/JAERI Collaborative Program on

Fusion Neutronics," *Fusion Technol.*, **19**, Suppl. B, 1891 (1991).

13. M. Z. YOUSSEF, Y. WATANABE, A. KUMAR, Y. OYAMA, and K. KOSAKO, "Analysis for the Simulation of a Line Source by a 14 MeV Moving Point Source and Impact on Blanket Characteristics: The USDOE/JAERI Collaborative Program on Fusion Neutronics," *Fusion Technol.*, **19**, Suppl. B, 1843 (1991).

14. T. NAKAMURA et al., "A Line D-T Neutron Source Facility for Annular Blanket Experiment: Phase III of the JAERI/USDOE Collaborative Program on Fusion Neutronics," *Fusion Technol.*, **19**, Suppl. B, 1873 (1991).

15. Y. OYAMA et al., "Annular Blanket Experiment Using a Line DT Neutron Source: Phase IIIA of the JAERI/USDOE Collaborative Program on Fusion Neutronics," *Fusion Technol.*, **19**, Suppl. B, 1879 (1991).

16. Y. OYAMA et al., "Concept and Characteristics of a Simulated Line Source for Annular Blanket Experiments Using an Accelerator-Based Deuterium-Tritium Neutron Source," *Fusion Technol.*, **28**, 305 (1995).

17. C. KONNO et al., "Neutronics Integral Experiments of Annular Blanket System Simulating Tokamak Reactor Configuration," *Fusion Technol.*, **28**, 347 (1995).

18. Y. OYAMA et al., "Phase III of the JAERI/USDOE Collaborative Program on Fusion Blanket Neutronics-Line Source and Annular Blanket Experiments – Volume I: Experiment," JAERI-M-94-015, Japan Atomic Energy Research Institute (Feb. 1994); see also M. Z. YOUSSEF et al., UCLA-FNT-75, UCLA-ENG-93-85, University of California, Los Angeles (1995).

19. M. Z. YOUSSEF et al., "Phase III of the JAERI/USDOE Collaborative Program on Fusion Blanket Neutronics-Line Source and Annular Blanket Experiments – Volume II: Analysis" (to be published as a University of California/Japan Atomic Energy Research Institute Joint report) (1995).

20. C. KONNO et al., "Measurements of the Source Term for Annular Blanket Experiment with a Line Source: Phase IIIA of the JAERI/USDOE Collaborative Program on Fusion Neutronics," *Fusion Technol.*, **19**, Suppl. B, 1885 (1991).

21. Y. OYAMA et al., "Phase-III Experimental Results of JAERI/USDOE Collaborative Program on Fusion Neutronics," *Fusion Eng. Des.*, **18**, 203 (1991).

22. W. A. RHOADES and R. L. CHILDS, "An Updated Version of the DOT 4 (Version 4.3) One-and-Two-Dimensional Neutron/Photon Transport Code," ORNL-5851, Oak Ridge National Laboratory (Apr. 1982); see also CCC-429, Radiation Shielding Information Center (1982).

23. L. P. KU and J. KOLIBAL, "RUFF – A Ray Tracing Program to Generate Uncollided Flux and First Collision Source Moments for DOT4, A User's Manual," EAD-R-16, Plasma Physics Laboratory, Princeton University (1980).

24. R. A. MacFARLANE, "TRANSX-CTR: A Code for Interfacing MATXS Cross-Section, Libraries to Nuclear Transport Codes for Fusion Systems Analysis," LA-9863-MS, Los Alamos National Laboratory (Feb. 1984).

25. "DOT 3.5: Two-Dimensional Discrete Ordinates Radiation Transport Code," CCC-276, Radiation Shielding Information Center; see also W. A. RHOADES and F. R. MYNETT, "The DOT III Two-Dimensional Discrete Ordinates Transport Code," ORNL-TM-4280, Oak Ridge National Laboratory (Sep. 1973).

26. M. NAKAGAWA and T. MORI, "MORSE-DD, A Monte Carlo Code Using Multigroup Double Differential Form Cross-Sections," JAERI-M84-126, Japan Atomic Energy Research Institute (July 1984).

27. M. NAKAGAWA, T. MORI, and M. SASAKI, "Comparison of Vectorization Methods Used in a Monte Carlo Code," *Nucl. Sci. Eng.*, **107**, 58 (1991).

28. M. Z. YOUSSEF, A. KUMAR, M. A. ABDOU, Y. OYAMA, K. KOSAKO, and T. NAKAMURA, "Post-Analysis for the Line Source Phase IIIA Experiments of the USDOE/JAERI Collaborative Program on Fusion Neutronics," *Fusion Eng. Des.*, **18**, 265 (1991).

29. M. Z. YOUSSEF et al., "Fusion Integral Experiments and Analysis and the Determination of Design Safety Factors – II: Application to the Prediction Uncertainty of Tritium Production Rate from the U.S. DOE/JAERI Collaborative Program on Fusion Blanket Neutronics," *Fusion Technol.*, **28**, 388 (1995).

30. M. Z. YOUSSEF, A. KUMAR, M.A. ABDOU, Y. OYAMA, and H. MAEKAWA, "Fusion Integral Experiments and Analysis and the Determination of Design Safety Factors – I: Methodology," *Fusion Technol.*, **28**, 366 (1995).

31. M. Z. YOUSSEF, A. KUMAR, and M. ABDOU, "The Prediction Capability for Tritium Production and Other Reaction Rates in Various Systems Configurations for a Series of the USDOE/JAERI Collaborative Fusion Blanket Experiments," *Fusion Eng. Des.*, **18**, 407 (1991).

32. M. Z. YOUSSEF et al., "Nuclear Analysis of Integral Experiments on a Li_2O Test Assembly with Local Heterogeneities Utilizing a 14-MeV Neutron Source," *Fusion Technol.*, **28**, 243 (1995).

33. M. Z. YOUSSEF and Y. OYAMA, "Required Design Margins and Their Economic Impact in Fusion Reactors to Compensate for Nuclear Data Uncertainties – A Global Approach to Define Safety Factors Based on Integral Experiments," *Proc. Int. Conf. Nuclear Data for Science and Technology*, Gatlinburg, Tennessee, May 9–13, 1994.

34. Y. OYAMA et al.,"Influence of Selection of Calculation Parameters in Discrete Ordinate Code DOT3.5 for Analysis of Fusion Blanket Integral Experiments in JAERI/USDOE Collaborative Program," *Fusion Eng. Des.*, **28**, 636 (1995).

Mahmoud Z. Youssef (PhD, nuclear engineering, University of Wisconsin, 1980) is a senior research engineer in the Department of Mechanical, Aerospace, and Nuclear Engineering at the University of California, Los Angeles (UCLA). He participated in several conceptual magnetic fusion energy and inertial fusion energy reactor design studies with emphasis on nuclear analysis and blanket/shield design. His research interests are in the areas of blanket/shield design optimization, nuclear data, sensitivity/uncertainty studies, neutronics methods and code development, tritium fuel cycle, radioactivity and safety aspects of fusion, integral experiments, neutronics testing, and research and development for fusion reactors, particularly the International Thermonuclear Experimental Reactor (ITER).

Mohamed A. Abdou is a professor in the Department of Mechanical, Aerospace, and Nuclear Engineering at UCLA and also is the director of fusion technology at UCLA. His research interests include neutronics, thermomechanics, fusion technology, and reactor design and analysis. He served as the U.S. leader of the Japan Atomic Energy Research Institute (JAERI)/U.S. Department of Energy (U.S. DOE) collaboration on fusion blanket neutronics.

Anil Kumar (PhD, University of Bombay, India, 1981) is senior development engineer at UCLA. His current research interests include fusion reactor nucleonics experiments and analysis, technique development for nuclear heating, decay heat measurements, biological dose, fusion diagnostics, safety factor methodology for fusion reactor design parameters, low-activation materials, inertial confinement fusion, and sequential reactions. He has conducted experiments at leading facilities such as the Fusion Neutronics Source (FNS) facility in Japan, the Tokamak Fusion Test Reactor (TFTR) at Princeton University, and LOTUS in Switzerland.

L. Zhang (graduate student, PhD candidate, UCLA) has a major research interest in fusion neutronics, particularly code development for nuclear heating calculations and kerma factor evaluation.

Kazuaki Kosako (BE, atomic engineering, Tokai University, Japan, 1984) has worked at Sumitomo Atomic Energy Industries since 1994. He worked in the Department of Reactor Engineering at JAERI from 1984 to 1992 where he was involved mainly in fusion neutronics. He is currently interested in the area of radiation damage of materials.

Yukio Oyama (BS, physics, 1975; MS, nuclear physics, 1977; and Dr. Eng., 1989, Osaka University, Japan) is a principal scientist at JAERI. He has worked in the area of fusion neutronics experiments since 1978. He is currently involved in intense and high-energy neutron source projects.

Fujio Maekawa (MS, nuclear engineering, Osaka University, Japan, 1990) is a research scientist at JAERI. He has been engaged in integral experiments for fusion neutronics and studied the behavior of neutron, photon, and electron transport in media. His current interests are in the measurements of tritium and decay heat of irradiated materials.

Yujiro Ikeda (PhD, nuclear engineering, Nagoya University, Japan, 1981) is head of the Fusion Neutronics Laboratory in the Department of Reactor Engineering at JAERI. He has worked in the areas of fusion neutronics experiments, induced radioactivity experiment and analysis, direct nuclear heating measurements, activation cross-section measurements, and fusion dosimetry.

Chikara Konno (MS, physics, Kyoto University, Japan, 1985) is a research scientist in the Department of Reactor Engineering at JAERI. He has worked in the areas of fusion neutronics experiments, cross-section measurements, and neutron spectrum measurements using a proton-recoil counter.

Hiroshi Maekawa (BE, 1965; MS, 1967; and Dr. Eng., 1970, nuclear engineering, Tokyo Institute of Technology, Japan) is the deputy director of the Department of Reactor Engineering and the head of the Intense Neutron Source Laboratory at JAERI. He has worked on fusion neutronics for more than 20 years, and he planned and constructed the FNS facility. He served as the Japanese leader of the JAERI/U.S. DOE collaboration on fusion blanket neutronics. His recent research has focused on International Fusion Materials Irradiation Facility conceptual design activities.